



HAL
open science

Orbital forcing and abrupt events in a continental weathering proxy from central Europe (Most Basin, Czech Republic, 17.7–15.9 Ma) recorded beginning of the Miocene Climatic Optimum

T. Matys Grygar, K. Mach, P. Schnabl, Mathieu Martinez, C. Zeeden

► To cite this version:

T. Matys Grygar, K. Mach, P. Schnabl, Mathieu Martinez, C. Zeeden. Orbital forcing and abrupt events in a continental weathering proxy from central Europe (Most Basin, Czech Republic, 17.7–15.9 Ma) recorded beginning of the Miocene Climatic Optimum. *Palaeogeography, Palaeoclimatology, Palaeoecology*, 2019, 514, pp.423-440. 10.1016/j.palaeo.2018.10.034 . insu-01921682

HAL Id: insu-01921682

<https://insu.hal.science/insu-01921682>

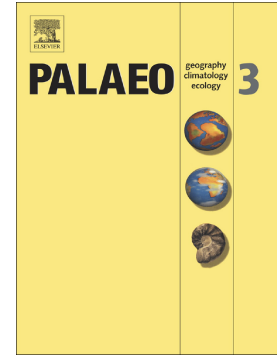
Submitted on 14 Nov 2018

HAL is a multi-disciplinary open access archive for the deposit and dissemination of scientific research documents, whether they are published or not. The documents may come from teaching and research institutions in France or abroad, or from public or private research centers.

L'archive ouverte pluridisciplinaire **HAL**, est destinée au dépôt et à la diffusion de documents scientifiques de niveau recherche, publiés ou non, émanant des établissements d'enseignement et de recherche français ou étrangers, des laboratoires publics ou privés.

Accepted Manuscript

Orbital forcing and abrupt events in a continental weathering proxy from Central Europe (Most Basin, Czech Republic, 17.7–15.9Ma) recorded beginning of the Miocene Climatic Optimum



T. Matys Grygar, K. Mach, P. Schnabl, M. Martinez, C. Zeeden

PII: S0031-0182(18)30576-5
DOI: <https://doi.org/10.1016/j.palaeo.2018.10.034>
Reference: PALAEO 8976

To appear in: *Palaeogeography, Palaeoclimatology, Palaeoecology*

Received date: 27 June 2018
Revised date: 27 October 2018
Accepted date: 31 October 2018

Please cite this article as: T. Matys Grygar, K. Mach, P. Schnabl, M. Martinez, C. Zeeden, , Orbital forcing and abrupt events in a continental weathering proxy from Central Europe (Most Basin, Czech Republic, 17.7–15.9 Ma) recorded beginning of the Miocene Climatic Optimum. *Palaeo* (2018), <https://doi.org/10.1016/j.palaeo.2018.10.034>

This is a PDF file of an unedited manuscript that has been accepted for publication. As a service to our customers we are providing this early version of the manuscript. The manuscript will undergo copyediting, typesetting, and review of the resulting proof before it is published in its final form. Please note that during the production process errors may be discovered which could affect the content, and all legal disclaimers that apply to the journal pertain.

Orbital forcing and abrupt events in a continental weathering proxy from central Europe (Most Basin, Czech Republic, 17.7-15.9 Ma) recorded beginning of the Miocene Climatic Optimum

T. Matys Grygar (1,*), K. Mach (2), P. Schnabl (3), M. Martinez (4), C. Zeeden (5)

(1) Institute of Inorganic Chemistry, AS CR, v.v.i., 250 68 Řež, Czech Republic

(2) North Bohemian Mines, j.s.c., 5. května 2013, 418 01, Bílina, Czech Republic

(3) The Czech Academy of Sciences, Institute of Geology, Prague, Czech Republic

(4) Univ Rennes, CNRS, Géosciences Rennes, UMR 6118, 35000 Rennes, France

(5) IMCCE, Observatoire de Paris, PSL Research University, CNRS, Sorbonne Universités, UPMC Université Paris 06, Université Lille, 75014 Paris, France

* corresponding author, grygar@iic.cas.cz

Abstract

We describe orbital forcing in siliciclastic lacustrine sediments, deposited in central Europe (ca. 50.5 °N and 13.5 °E, the Most Basin, the Czech Republic) between ~17.7 and ~15.9 Ma, i.e., before the Miocene climatic optimum (MCO) and in its early stage. Chemical element analysis combined with magneto- and cyclostratigraphy produced a consistent stratigraphy for the studied basin fill. The palaeoenvironmental record is mainly based on variations of the chemical weathering intensity in the lake catchment (normalised potassium concentration K/Al or K/Ti). The Most Basin sedimentary profile is specific by relatively high deposition rates (typically 20 cm/kyr, sampling density corresponded to temporal resolution of 1-2 kyr) and sensitivity to a regional continental climate. For age control, we used the ATNTS2012 for younger sediments and an alternative age of the onset of C5Dn chron and the end of C5Dr.1r short chron. In the earliest studied interval, the chemical weathering intensity in the catchment was controlled by precession, while between 17.5 and 17.15 Ma, short eccentricity was mainly driving chemical weathering intensity. After 17.05 Ma, i.e., just before the onset of the MCO, and in the period of persistent high eccentricity between 16.95 and 16.7 Ma, chemical weathering intensity reached its precession-controlled maxima. In the subsequent period of the persistent low eccentricity at 16.65 Ma, the orbital signal nearly vanished in the Most Basin. Abrupt but temporary environmental change occurred in the interval between 16.5 and 16.35 Ma (polarity chron C5Cn.2n), within two cycles of high eccentricity. Its trigger is uncertain but it might have been local or regional. The obtained composite record was compared with marine $\delta^{13}\text{C}$ and $\delta^{18}\text{O}$ data, showing certain global control of the Most Basin deposits. The Most Basin record thus shows

climatic events of the pre-MCO and early MCO period in terrestrial settings of Central Europe, with changes at 17.05, 16.65, and 16.5 Ma, possibly representing triggers of the MCO.

Keywords: geochemistry; eccentricity; precession; polarity time scale; Miocene; continental weathering

1 Introduction

The research of the Neogene climate dynamics has proliferated mainly from long and continuous datasets of climate proxies from marine pelagic sediment cores (e.g. Flower and Kennett, 1994; Zachos et al., 2003; Tian et al., 2008; Liebrand et al., 2017), extension of the astronomical solution back in time (Laskar et al., 2004), and improvements in integrated stratigraphy (Kuiper et al., 2008; Hilgen et al., 2012). Pelagic (marine) sedimentary archives have a good preservation potential, continuity, and common deposition rates in order of mm/kyr to cm/kyr. Variations in the sediment composition and its carbon and oxygen stable isotopes have been controlled by global oceanic circulation patterns (e.g., Flower and Kennett, 1994; Holbourn et al., 2014), polar ice volume (Liebrand et al., 2017), and varying atmospheric circulation patterns such as monsoon intensities (Clift et al., 2014). Continental and near-shore marine archives (Utescher et al., 2012; Valero et al., 2014, 2016, 2017, Levy et al., 2016; Marshall et al., 2017) have yet been studied less extensively, although the knowledge on continental expression of climate changes is relevant for a complete understanding of the past climate dynamics. Continental and near-shore marine archives are, however, strongly influenced by local palaeogeography, tectonics, and sediment reworking under dynamic depositional environments thus need very careful interpretation and demanding stratigraphic work (Abels et al., 2010, 2013; Valero et al., 2014, 2017; Uličný et al., 2014; Marshall et al., 2017). Their advantages are often higher deposition rates and a better temporal resolution. The complexity of continental archives is a challenge even for so large and extensively investigated basins as the North Alpine Foreland Basin (Reichenbacher et al., 2013) and the Paratethys area (e.g., Sant et al., 2017b).

The Miocene climatic optimum (beginning at ~16.9 Ma) and a subsequent Miocene climatic transition (MCT, 15.8-12.5 Ma) are among the most dramatic recent global climate changes (Flower and Kennett 1994) and associated biotic turnovers (Böhme, 2003). They were coupled with substantial variations of the Antarctic ice sheet extent (Passchier et al., 2011; Levy et al., 2016), the driving of which is yet poorly understood. The continental impact of the MCO is yet elusive (Utescher et al., 2012; Kotthoff et al., 2014). Although dating of the MCO-related climatic events has recently been improved considerably, the MCO triggers remain uncertain (see discussion in Armstrong McKay et al., 2014). Holbourn et al. (2015) and Mahood and Benson (2017) discussed the main challenges of the hypothesis by Courtillot and Renne (2003), suggesting that the MCO was related to the formation of

the Columbia River Basalt Group (CRBG). Firstly, as in the case of other magmatic traps, the question remains whether the total amount of CO₂ liberated by CRBG magma degassing was sufficient to cause polar ice melting (Armstrong M^cKay et al., 2014). Secondly, the first CRBG lava flows post-dated the onset of the MCO by ~0.2 Myr (Baksi 2012; Mahood and Benson 2017). Moreover, even before the MCO, shoaling of the carbonate compensation depth in the equatorial Pacific Ocean at ca. 18.5-16 Ma was found (Pälike et al., 2012; Channell et al., 2013) and the Antarctic ice sheet intermittently melted already at ca. 17.6-17.8 Ma (Passchier et al., 2011; Levy et al., 2016). De Vleeschouwer et al. (2017) have recently shown substantial changes in the insolation feedback before, during, and after the MCO. Possibly the Earth system approached several environmental thresholds at ~18 Ma, including variable altitude of the Antarctic ice sheet due to persistent glacial abrasion of the continent (Gasson et al., 2016; Levy et al., 2016), complicating a straightforward identification of the MCO triggers. Sedimentary archives of the pre-MCO and MCO periods thus remain an attractive study.

The detailed studies of the pre-MCO and early MCO environmental events face a problem of uncertainties in time scales and dating. There are several magnetic polarity time scales for the interval relevant for our Most Basin study (Billups et al., 2004; Hilgen et al., 2012; Kochhann et al., 2016). The longest continuous Neogene time scale (ATNTS2012) is a composite record, in which the dating in the interval 15-23 Ma was obtained from a model of seafloor-spreading-rate history with limited orbital tuning (Hilgen et al., 2012). Other time scales from that period are shorter, but orbitally tuned (mostly to eccentricity cycles) records have been obtained from the equatorial Pacific Ocean (Kochhann et al., 2016) and south-eastern Atlantic Ocean (Liebrand et al., 2016). In the equatorial Pacific Ocean, Channell et al. (2013) found inconsistencies with ATNTS2004 in duration of C5Cn.1r (~16.2 Ma) and three preceding chrons. For the same reason, Ohneiser et al. (2013) did not use the ATNTS and preferred an alternative time scale for chrons older than C5Br (base ~16.0 Ma). Kochhann et al. (2016) found different timing compared to ATNTS2012 for polarity reversals C5Cn.3n (~16.7 Ma) and older. Hiatuses (due to dissolution) in pelagic carbonate sediments at ~17.0 Ma were identified by Wu et al. (2014) and at 17-18 Ma by Miller et al. (2017). Those hiatuses or horizons with low deposition rates were attributed to the changes in the carbonate compensation depth, which probably resulted from changes in ocean circulation and atmospheric CO₂ concentration related to the MCO onset. In the period from 17.5 to 16.7 Ma, Kamikuri and Moore (2017) recognized a “carbonate famine” due to changes in the Pacific Ocean water upwelling at ca. 17.0 Ma. As a consequence of preceding facts, overall uncertainty of the early Miocene time scale can be estimated to <100 kyr. This uncertainty is comparable to the uncertainty in the ⁴⁰Ar/³⁹Ar dating for the same period due to the inaccuracy of the primary standard for this method (Kuiper et al., 2008; Hilgen et al., 2012; Phillips and Matchan, 2013; Mahood and Benson, 2017). Here orbital tuning can clearly contribute to time scale development.

One sedimentary archive of the pre-MCO and MCO period was formed in central Europe in a basin-wide lake that existed between ca. 17.7 and 15.9 Ma in the Most Basin (Fig. 1), the north-western part of the Czech Republic (Matys Grygar et al., 2014, 2017b) and in its underlying strata (Matys Grygar et al., 2017a). Geochemical and spectral analyses combined with magnetic polarity stratigraphy in the Most Basin sediments (Matys Grygar et al., 2014, 2017a, 2017b) produced the record shown in Fig. 2. The mean rate of sediment deposition in the Most Basin was ~20 cm/kyr (Fig. 2). The major K/Ti minima in the lower part of the record in Fig. 2 are broad, slightly asymmetrical, with gradually descending and ascending sides similar as the eccentricity-controlled variations in geochemical proxies for global ice sheet extent in the late Oligocene/early Miocene (Liebrand et al., 2017). Similarly, as Zabel et al. (2001), Clift et al. (2014), and Wan et al. (2017), we assigned the K or K/Ti minima in the Most Basin sediments to the maximal intensity of chemical weathering in the source area (Matys Grygar et al., 2017b). This interpretation is further corroborated in this paper. One may expect that every weathering intensity proxy should mirror climatic development. Indeed, in the K/Ti depth profile of the HK591 plot using the ATNTS2012 timing of the polarity reversals (Hilgen et al., 2012) we found a match between major K minima and eccentricity maxima in the upper part of the Libkovice Member, but a less straightforward relation in the lower parts of those cores (Fig. 2). A similar misfit was also found in the lower part of the HD50 core laterally correlated with HK591 (Matys Grygar et al., 2017a), showing a possible principal problem in sediment dating. There are two possible explanations of that misfit: variable deposition rate in the Most Basin and uncertainty in polarity time scales discussed above.

The aims of this work were to (a) improve the existing age model for the Most Basin deposits based on magnetic polarity reversals, in particular clarify discrepancies in dating the early clastic deposition in the Most Basin (Fig. 2, discussion in Matys Grygar et al., 2017a), (b) verify the depth-age model in the uppermost deposits by magnetic polarity analysis, yet missing (Matys Grygar et al., 2017b), (c) discuss the geochemical and orbital patterns in sediment geochemistry, and (d) compare the Most Basin record to regional and global records based on IODP studies (Holbourn et al., 2015; Kochhann et al., 2016; Miller et al., 2017). This study adds data from two drill cores, DO565 and OS17 to previously published data. The individual marine records may have been impacted by changes in the carbonate compensation depths (Miller et al., 2017), and we thus decided to date environmental events of the pre-MCO period in non-marine environment of the Most Basin. Compared with previous work (Matys Grygar et al., 2017b) we hereafter addressed discrepancies in polarity time scales in the pre-MCO period and uncertainties in dating the pre-MCO and early MCO climatic events; here the Most Basin record might contribute due to its insensitivity towards disruptions of the global carbon cycle, which resulted in issues for marine records.

2 Study area and methods

2.1 Study area

The Most Basin is a half-graben structure within the Ohře Rift in the Czech Republic (Rajchl et al., 2009; Fig. 1) with deposits preserved in an area of ~870 km² (Kvaček et al., 2004). Its Oligocene volcanogenic surface (mainly mafic effusive rocks) was first shaped by fluvial systems. In the early Miocene the basin floor was covered by peatlands with local water bodies, and later by a basin-wide freshwater lake (Mach et al., 2014). The formerly thick lava cover around the basin floor was eroded under a climate warmer and more humid than today (Mach et al., 2014), that allowed for deep weathering of rocks to illite-smectite and kaolinite. Weathering of mafic lavas under subtropical (von Eynatten et al., 2016) and tropical climates (Ryan and Huertas, 2009) are thus good analogues for the part of the Most Basin catchment, due to their similarity of climate and geology. A geographically more remote, but relevant from geochemical point of view, part of the catchment extended far south of the Most Basin and included older deposits of Palaeozoic basins and metamorphic rocks of the Bohemian Massif (Mach et al., 2014).

The here relevant stratigraphy of the resulting Most Basin sedimentary fill is shown in Fig. 3. It includes an approximately 30 m thick coal seam (the main coal seam) and its clastic lateral equivalents (fluvial and local lacustrine deposits), all assigned as the Holešice Member. The coal was formed in prevalently coniferous swamps with *Glyptostrobus* and *Quasisequoia* trees broadly resembling extensive modern *Taxodia* wetlands in the south-east of the USA. In the Bílina area, a shallow (local) lake existed before ca. 17.7 Ma within the wetlands, of which clastic sediments have a total thickness up to ca. 130 m near the Bílina Mine area (Matys Grygar and Mach 2013). That local lake was formed due to a combination of the basin floor subsidence and gravitational compaction of the underlying peat (Matys Grygar et al., 2017a). Above the Bílina (local) lake deposits, as well as above the main coal seam elsewhere in the basin, there is an up to ~300 m thick sequence of clastic sediments. This includes basin-wide lacustrine deposits of the Libkovice Member and in places erosional remnants of the Lom and Osek members.

The deposition of monotonous silty-clayey lacustrine sediments was interrupted by about 15 m thick laterally variegated deposits of the Lom Member with thin (less than 1 m) coal seams embedded in coaly clays; the organic matter was formed from a mixture of aquatic and terrestrial plants in a prevalently lacustrine environment (Havelcová et al., 2015). The subsequent Osek Member consists of lacustrine sediments geochemically and texturally resembling those of the Libkovice Member. The basin remained flow-through with major outflow to the north-west *via* NW European Tertiary basins to the North Sea. Only during the deposition of the Lom and Osek members, the palaeogeography might have changed to clastic input from NW and outflow to NE (Mach et al., 2014).

Palaeontologists assigned the Most Basin fill to the Burdigalian age, based on the identification of the small mammalian biozone MN3 found at the base of the main coal seam (Fejfar and Kvaček, 1993; Kvaček et al., 2004; Mach et al., 2014). The lacustrine sediments (the Libkovice and Osek members) are practically fossil barren.

The sediments of the Libkovice Member can be laterally correlated over the entire basin using the local chemostratigraphic scheme based on variations of mineral/element composition (Matys Grygar and Mach 2013; Matys Grygar et al., 2014, 2017a, 2017b). The mineral/geochemical composition of the Most Basin lacustrine sediments was partly orbitally controlled (Matys Grygar et al., 2014, 2017a, 2017b). Several drill cores were subject to spectral and magnetic polarity analyses (Matys Grygar et al., 2014, 2017a, 2017b), which refined their dating to the upper Burdigalian.

2.2 Element proxies for mineral composition and grain size of sediments

The mineralogical composition of the Most Basin sediments was studied by previously published X-ray diffraction analyses (Matys Grygar and Mach, 2013; Matys Grygar et al. 2017a; and references therein). The Most Basin lacustrine sediments (Libkovice and Osek members) are composed of clay and silt-sized detritus, namely several populations of illite-smectite interstratified clay mineral (I/S) of variable I to S proportions, possibly accompanied by kaolinite-smectite (K/S), kaolinite, illite, and quartz (Matys Grygar et al., 2017a) and autochthonous components, in particular siderite and minor but important crandallite, Sr-Ca aluminophosphate, and a member of the alumina-phosphate-sulphate group of minerals (Dill 2001). We have identified three crandallite horizons in the Libkovice Member (C1-C3; Matys Grygar et al., 2014, 2017b), these are always found within the same position in specific K minima. These horizons are laterally correlated across the basin (Fig. 3). The variations in the mineral proportions in sediments are sensitively reflected by the element composition, which is accessible by X-ray fluorescence analysis at a sampling resolution sufficient for identification of orbital signatures.

The element composition of geochemically mature sediments reflects mainly sediment grain size (Al/Si, Bouchez et al., 2011; Matys Grygar and Popelka, 2016; von Eynatten et al., 2016; Liu et al., 2017), chemical weathering intensity (K content, Zabel et al., 2001, Clift et al., 2014; Wan et al., 2017, Matys Grygar et al., 2017b, Molliex et al., 2017), and the past (micro)environments in the sediment-water interface (chemogenic components, here Fe and Sr minerals). The Al/Si ratio in mature sediments is proportional to the content of clay minerals, in particular in the Most Basin kaolinite (Al/Si=1) relative to quartz (Al/Si=0; Bouchez et al., 2011; Matys Grygar and Popelka, 2016; Xu et al., 2018). Zr/Rb is used as a proxy for coarser silt and finest sand (Chen et al., 2006; Xu et al., 2018), because those size fractions contain most zircon crystals, and Rb is mostly carried by clay-size illite in mature sediments, and is interstratified with illite-smectite minerals.

2.3 Sampling, analytical methods, and datasets available for this work

The position of cores dealt with in this paper is shown in Fig. 1. We reused or revisited datasets obtained for drill cores HD50, HK591, and HK772 and described in detail in several previous papers (Matys Grygar and Mach 2013; Matys Grygar et al., 2014, 2017a, 2017b). We also newly sampled and analysed the magnetic polarity and element composition of the DO565 core, starting with the top of the Holešice Member. We also analysed the OS17 drill core, covering the Lom and Osek members. The clastic deposits of the Holešice and Libkovice members were examined in numerous cores from distinct parts of the basin. Here all geochemical features discussed in this paper are correlated at the basin scale (Matys Grygar and Mach, 2013; Matys Grygar et al., 2014, 2017a), except for early stages of the basin fill, when local differences occur (Mach et al., 2014; Matys Grygar et al., 2017a). The Lom and Osek members were acquired in the erosion remnants of the basin fill; those strata were thus obtained in only 2 cores, with a distance of less than 0.4 km.

To support magnetic polarity analyses above the main coal seam in the Tušimice Mine area, we performed manual sampling in the hanging walls (DRP profile) for comparison with the cores.

Element analysis of DO565 and OS17 was performed by energy dispersive X-ray fluorescence spectroscopy (XRF) using Epsilon 3^X (PANalytical, the Netherlands). As in our previous studies, the analysis was performed on loose powdered sediments (Pulverisette planetary micromill, Fritsch, Germany) in PANalytical measuring cells with Mylar foil bottoms. The analytical signals were calibrated using certified reference materials CTA FFA-1 provided by the Institute of Nuclear Chemistry and Technology (Warsaw, Poland), SL-1, SL-3, and 314 by IAEA (Vienna, Austria), Metranal 31 and 34 by Analytika, s.r.o. (Prague, the Czech Republic), and 1646a, 2702, 2704, and 2711a by NIST (the USA). To limit the dilution effects by variable contents of quartz and siderite and grain-size effects, we normalised the K concentrations to Al or Ti, i.e., we expressed the K content as concentration ratio to those reference elements. The normalisation by Ti (also shown in Fig. 2) has been successfully used in the Libkovice Member (Matys Grygar et al., 2014), while in the Holešice Member in the central and northern part of the basin, titanium acted not only as the grain-size normaliser but it was partly governed by changes in the palaeogeographic development in the early stages of the massive Miocene fill (Elznic et al., 1998, Mach et al., 2014; Matys Grygar et al., 2017a) and Ti normalisation is thus less efficient for lateral correlations. Beside geochemical substantiation of normalisation (Matys Grygar and Popelka, 2016), evaluation of the element ratios instead of raw element concentrations (for elements with similar XRF analytical lines) improves robustness of the XRF determination against spectral and matrix interferences.

Cation exchange capacity of sediments (CEC) was determined using Cu²⁺ complex with triethylenetetramine (trien) ligand (Meier and Kahr, 1999; Grygar et al., 2009). The results were

expressed as ΔCu , the amount of Cu^{2+} ions consumed for ion exchange in mmol/g. ΔCu of pure smectite would be ~ 0.5 mmol Cu^{2+} /g and kaolinite ~ 0.01 mmol Cu^{2+} /g. In sediment profiles we used CEC in the form of identification of the CEC step (Fig. 3).

Magnetic polarity analyses for HK591 were published by Matys Grygar et al. (2014) and revisited by Matys Grygar et al. (2017b). For the HD50 core it was published in Matys Grygar et al. (2017a) with some misfits in the lower part of the core. The DO565 and OS17 polarity analyses were newly performed analogously as for previous core analyses. Typically, one specimen per meter was sampled for palaeomagnetic analyses within one week after coring. The remanent magnetization and alternate field (AF) demagnetization was performed on a Type 755 4K SRM superconducting rock magnetometer (William S. Goree, Inc., Sand City, CA). The AF measurement consisted of 11 to 15 demagnetization steps from 0 to 50 mT, the demagnetisation step was between 3 and 10 mT. The individual components of the magnetization were determined by principal component analysis (Kirschvink, 1980) using the Remasoft software package (Agico, Brno, the Czech Republic).

2.4 Depth-age conversion

We previously proposed depth-age relationships (Matys Grygar et al., 2014, 2017a, 2017b) based on the magnetic polarity reversals according to the ATNTS2012 combined with the examination of orbital patterns in geochemical composition. The relative K contents and Al/Si ratios in the lacustrine sediments of the Most Basin formations reflect mainly short eccentricity and precession cycles (Matys Grygar et al., 2014, 2017b). The amplitude of that forcing was considerably weakened or disappeared in favour of orbital tilt in the eccentricity minimum/node around a particularly low-amplitude short eccentricity minimum near 17 Ma, which supports the depth-age relationship (Matys Grygar et al., 2014) as this pattern can be observed in other reference datasets as well. Examination of geochemical datasets on an age scale and their comparison with astronomical solution (Laskar et al., 2004) showed rough coincidence of the eccentricity maxima and K minima in the Most Basin sediments, except for the lowermost part of HK591 (Fig. 1) and HD50 (Matys Grygar et al., 2017a). In the newly constructed geochemical composite curve for the Most Basin, we verified the depth-age model for lower part of HK591 core with coarser deposits of the Bílina delta (Matys Grygar et al., 2017b) using HD50 core with lithologically uniform fine off-shore sediments (Matys Grygar et al., 2017a).

In the HD50 and HK591 drill cores, we found a misfit between results of cyclo- and magnetostratigraphy when we used polarity reversal dating according to the ATNTS2012 (Matys Grygar et al., 2017a). Due to expected uncertainty of the ATNTS2012 polarity time scale in intervals where orbital tuning has not been applied (see also discussion in Turco et al., 2017), we revisited the age model for those two quoted cores.

Spectral analysis, i.e., the identification of orbital cycles in the geochemical dataset, was performed using conventional tools as described in previous papers (Matys Grygar et al., 2014, 2017a, 2017b). Eccentricity tuning was performed manually by fitting the K depth profiles to the eccentricity maxima from the Laskar (2004) orbital solution. The ages between the K minima were produced by linear or polynomial interpolation. To compare the orbital imprints as derived from several depth-age models with the Laskar (2004) orbital solution, we used the 'testPrecession' method (Meyers, 2014; Zeeden et al., 2015; R core team 2017). This test was applied to check whether eccentricity tuning enhances the expression of the precession signals, as would be expected in a correct eccentricity tuning. The test compares the precession amplitude modulation of geological data with the orbital template of Laskar et al. (2004). We tested both individual cores and the composite geochemical logs. Although precession (and obliquity) phases may not be correct in the La2004 solution (Laskar et al. 2004, Zeeden et al. 2014), the number of precession cycles per 100-kyr eccentricity cycle is reliable. Therefore, we do not expect problems working with the precession signal, although its phase is not reliable.

3 Results

3.1 Depth profiles and stratigraphic correlation of drill cores

Fig. 4 shows geochemical depth profiles of drill cores used in this study. The cores were laterally correlated using the stratigraphic scheme shown in Fig. 3, discussed in section 2. Mineral and element compositions of sediments are interrelated as described in section 2.2. Element proxies are used in the studied sediments due to their lithological uniformity. All drill cores with the lower part of the Libkovice Member can be correlated above the K2 minimum, and the CEC step horizon (Figs 3 and 4), i.e., above the boundary of the Holešice and the Libkovice members (green tie line in Fig 4). Unequivocal tie points correlate HK519 to HK772, and OS17 drill cores, based on element proxies characteristic for the end of the Libkovice Member (turquoise tie line in Fig. 4) and for the Lom Member (light brown tie line in Fig. 4).

Magnetic polarity zones may be assigned to chrons following previous work (Matys Grygar et al., 2014, 2017a, 2017b). The result is shown in Fig. 5. There are certain differences in thicknesses of the lowermost polarity zones, and intervals between the onset of the clastic deposits over the main coal seam with K1 minimum and the Holešice/Libkovice boundary near K2 minimum. Those differences are discussed hereafter.

3.2 Geochemical signatures in studied sediments

In the clastics of the Holešice Member in the first metres above the main coal seam, the trends of upward increasing Al/Si and decreasing of Zr/Rb point to decreasing content of coarse silt and fine sand (Fig. 6C). Then, the Al/Si decreases, while no change is observed in Zr/Rb ratio, suggesting that the contribution of clay in the whole rock remains constant while the kaolinite contribution in the clay mineral assemblage increases (decrease of Al/Si with no change in Zr/Rb, Figs 6A and 6C near K2 minimum). The mineralogical and grain-size changes in the subsequent lacustrine sediments (Libkovice Member) are much lower, not revealed by visual examination but discernible from the geochemical composition. Variations of K concentrations are most important, as their minima are laterally correlated and orbitally controlled (Matys Grygar et al., 2014, 2017a, 2017b; Fig. 4).

In the strata with variable fine sand and silt contents, such as in early lacustrine sediments near the Bílina delta (top of the Holešice Member), Al/Si is lower and Zr/Rb larger in strata containing more fine sand. Simultaneously, the K/Al ratio slightly decreases, showing a minor grain-size effect on the K content. This pattern is represented in K/Al minima K1, lower part of K3, lower part of K4 (Figs 6A and 6C), and three minima in P1 range (Fig. 6B). In sediment strata with stable grain sizes, Al/Si and Zr/Rb variations are small (less than 5 %) or indiscernible from noise, while K content (raw, or normalized to Al or Ti concentrations) shows clear minima (decrease by 10-20 % compared to depth intervals outside the minima) simultaneous with increased CEC. Such a pattern is best represented in the upper part of K2 (Fig. 6C) and most K minima in the interval P1 (Fig. 6B). These can be attributed to a variable proportion of smectitic and illitic structures in the sum of illite-smectite interstratified minerals. In this pattern, the K minima are coeval with Al/Si maxima and CEC minima, obviously a consequence of kaolinite prevalence over both illitic and smectitic structures. The best examples are the lower part of K3 and most remarkably in K5 (Fig. 6A). In summary, the K minima mark chemically more mature (more intensively weathered) sediment, perhaps in association with slightly coarser particles such as kaolinite and quartz in K5. In the geochemical data, these three patterns are combined in some K minima. As a weathering proxy, K concentrations can be expected to reflect the catchment climate.

The K minimum with the most atypical pattern is K5: it is associated with a sharp increase in Al/Si ratio and considerable grain size variation revealed by Zr/Rb maximum, i.e., kaolinite and quartz silts as two main constituents and relatively large amount of zircon (Fig. 6A). Crandallite horizon C2, probably formed on the few mm thick layer of volcanic ash (Novák et al., 1993), is at the sharp basis of the K5 minimum. Either it is a co-incidence, or K5 is genetically different from other K minima.

The geochemical variability is considerably lower in OS17 drill core (Fig. 6D) than in cores within the Libkovice Member (Figs 6A-6C). The most remarkable heterogeneity in OS17 is represented by the Lom Member with kaolinite-rich coaly deposits (remarkably high Al/Si and low K/Al, Fig. 6D). In the lacustrine sediments of the Osek Member, three K minima are present (P2 interval in Fig. 6D) in otherwise geochemically monotonous deposits.

3.2 Revised depth-age model for core HD50

The cores HD50 and HK591 originate in the Bílina Mine area and their geochemical logs may easily be laterally correlated (Fig. 4). The coarse silt/fine sand strata disturbing the basis of the lacustrine sequence in HK591 (sharp Al/Si minimum at depth of ca. 205 m in Fig. 4) are absent in HD50. What is clear from the correlation in Fig. 4 is a varying thickness of the intervals between K1 and K2, and between K2 and K3 in HK591 and HD50. We assign this fact to laterally variable deposition rates, which may be expected for the earliest stages of fluvio-lacustrine development of the former peat swamp. Spectral analysis of K/Ti in HD50 showed a ~30 m signal of short eccentricity and a ~6 m signal of precession (Matys Grygar et al., 2017a) in the middle and upper part of the core. The lower part of the core was not interpreted unequivocally in previous work (Matys Grygar et al., 2017a).

We tested two routes to refine the depth-age model for HD50: (1) replacing the ATNTS2012 polarity time scale (Hilgen et al., 2012) by an alternative time scale published by Kochhann et al. (2016) and (2) construction of eccentricity-tuned time scale based on assumption of association of K minima and eccentricity maxima observed in the upper part of the same core (Matys Grygar et al., 2017a, 2017b). The comparison of the K/Ti logs with orbital cycles in several depth-age models is shown in Fig. 7. The alternative time scale by Kochhann et al. (2016) produced better fits of K/Al minima and eccentricity maxima in the lower part of the core. We thus combined the ATNTS2012 (Hilgen et al., 2012) and the alternative time scale by Kochhann et al. (2016) as specified in Table 1. In some of these models, a good match of the found precession amplitude with the orbital template was found (orange tie lines Fig. 7).

To evaluate individual experimental time scales quantitatively, we used the ‘testPrecession’ algorithm (Zeeden et al., 2015), which is here used for testing the usefulness of the tuned time scales. We tested four depth-age models for the K/Al ratio in HD50 drill core: (1) based on ATNTS2012 magnetic polarity time scale, (2) based on magnetic polarity time scale by Kochhann et al. (2016), (3) combination of both preceding as shown in Table 2, and (4) eccentricity-matched model based on minimal manual tuning of the model (3) by wiggle matching the K/Al minima to the nearest eccentricity maxima. The age model (1) failed in the ‘testPrecession’, because precession amplitudes were negatively correlated to eccentricity. The age model (2) had P-value of 0.736 (insignificant), model (3) had p-value of 0.276 (significant at >70% probability). The model (4) obtained by eccentricity matching of the best of previous polarity-based models had P-value 0.054 (significance at >90%). This latest model was also used to estimate corresponding ages of polarity reversals (Table 2); those ages indeed confirm the combination of the existing polarity time scales. The timing of the onsets of C5Dr.1r and C5Dn in that tuned model are closer to those in the time scale by Kochhann et

al. (2016). One more argument supporting the age model for HD50 is based on the combined time scale. It is the weakening of short eccentricity and precession signals (observed in K/Al) in the eccentricity node at ~17.4 Ma (between the K2 and K3 minima).

3.3 Depth-age model for DO565 core

The obtained magnetic polarity and normalized K logs in DO565 are similar (can be correlated) with those obtained in HD50 core (ca. 35 km far from DO565). A normal magnetozone interpreted as C5Dn (Fig. 5) was deposited at a mean rate of 19 cm/kyr, using both polarity time scales (ATNTS2012; Kochhann et al., 2016 time scale). A short normal magnetozone in the first clastic deposits on the main coal seam in DO565 (roughly between the K1 and K2 minima, Fig. 4) was interpreted as C5Dr.1n subchron (Fig. 5). The normal magnetic polarity at the base of DO565 core was confirmed by the analysis of the DRP profile in the first few metres above the main coal seam and below K2 in the Tušimice Mine (not shown here). The mean deposition rate in the C5Dr.1r was only 10 cm/kyr according to polarity time scales (ATNTS2012) or 9 cm/kyr (Kochhann et al., 2016 time scale). This would imply a sedimentation rate decrease to about half between K2 and K4 minima.

Spectral analysis in DO565 (Fig. 8) identified 23 m (significant) and 4.9 m (non-significant) cycles in the K/Ti ratio between the K2 and K4 minima, which we interpret as short eccentricity and precession, respectively, analogously as in all other cores.

Aiming to refine the age model for the core including its lower part, eccentricity tuning was performed using minima K1 to K4 (Fig. 9A). Although 'testPrecession' did not find significant correlation, this cannot be interpreted as a wrong time scale. It is probably due to the rather short duration of the examined record. The precession signal is obviously present in the upper and lowermost parts of the core (Fig. 9B). Eccentricity matching produced a mean sedimentation rate between K2 and K4 of 17 cm/kyr, i.e., a value very similar to the 19 cm/kyr using polarity time scales. With the eccentricity-tuned depth-age model, the timing of the onset of the C5Dn chron in DO565 (Table 1) is close to the time scale by Kochhann et al. (2016).

3.4 Revised depth-age model for core HK591

Based on the revised and novel depth-age models for HD50 and DO565, we revised the interpretation of the magnetic polarity reversals in the lowermost part of core HK591, published previously (Matys Grygar et al. 2014, 2017b). We decided to omit 2 neighbouring samples with normal polarity at a depth of ~200 m, because these are very close to the flush of coarse silt/fine sand sediments of the Bílina delta (204-206 m), which do not preserve a reliable paleomagnetic signal. The

lowermost polarity zone in HK591 was thus re-interpreted as C5Dr.1n subchron, analogously to HD50 and DO565 (Fig. 5).

The eccentricity-tuned age model for the lower part of core HK591 is shown in Fig. 10A. The tuning allowed for extending the depth-age model downward in depth, and omitted the misfit shown in Fig. 2. The tuning was verified by visual correspondence of the K variability at a wavelength of 3 to 4 m, with the precession signal shown by orange tie lines in Fig. 9A, supported by the ‘testPrecession’ (Figs 10B and 10C). The ‘testPrecession’ is highly significant for both K/Al and K/Ti logs (K/Al: <0.03 , K/Ti: <0.05). The corresponding dating of polarity reversals is listed in Table 1; it is consistent with results obtained with HD50 and DO565 cores and close to the combined polarity time scale.

3.5 Depth-age model for OS17 core (Osek and Lom members)

We performed spectral analysis of the Al/Si and K/Al ratios in core OS17, but the results were inconclusive due to low variability of those element ratios in the Osek Member deposits, compared to the Libkovice Member (compare Fig. 6D with Figs 6A to 6C). Spectral analysis was, however, successful for the K/Ti ratio in the top 120 m of core OS17, i.e., the Osek Member (Fig. 11). The obtained frequencies (Fig. 11) suggest a mean sedimentation rate ca. 25 cm/kyr.

The results of magnetic polarity analysis in OS17 are shown in Fig. 12. Correlation to other cores was based on lithological and geochemical ties shown in Fig. 4. The assignment of the magnetic polarity zones to established magnetochrons is based on the mean deposition rate of the Osek Member of ~25 cm/kyr suggested by cyclostratigraphy. The long, normal magnetozone in the middle to upper parts of OS17 can only correspond to C5Dn.1n, the only sufficiently long normal polarity chron preceded by a series of relatively short subchrons, that existed before and around the Burdigalian/Langhian boundary.

The base of the OS17 core (the uppermost deposits of the Libkovice Member) was dated by extrapolation of the magnetic polarity-derived age model for the HK772 core (Matys Grygar et al., 2017b), and geochemical- and lithological correlation in cores OS17, HK772, and HK591 (Fig. 4). The lower part of OS17 core includes the facies-variable coaly deposits of the Lom Member, which are rich in organic matter and occasionally include pyrite-rich beds, both responsible for the elevated content of sulphur (Fig. 12). In those sediments, analogous to the coal-bearing parts, namely sulphur- and kaolinite-rich coal strata of the Holešice Member, magnetic polarity acquisition was not successful. This was probably due to reductive decay of the original magnetic carriers. We assume that for this reason we did not identify chron C5Cn.2r (Fig. 7).

The newly obtained magnetic polarity analysis confirmed the age-model for core OS17, also by identification of the reverse subchron C5Cn.1r in the lower part of the lacustrine deposits of the Osek Member (just above the Lom coal and clays). We could not extrapolate the mean deposition rate

in the thin magnetozone to the rest of the Osek Member, where no other reversal has been identified (in agreement with the ATNTS2012 time scale, Fig. 7). We thus used the mean deposition rate in the core from cyclostratigraphical analysis, and the centre of the subchron C5Cn.1r as fixed time point to obtain the depth-age model for OS17.

4 Discussion

4.1 Uncertainty of time scale in the Most Basin

The depth-age models developed (and refined) in this work were used for the construction of a composite geochemical record, see Fig. 13. The age model was obtained by the refinement of the magnetic polarity age model combining two existing time scales (Table 1), and performing an integrated approach using eccentricity tuning and a quantitative test (testPrecession; Figs 7, 9, and 10). We found that the astronomically tuned time scale by Kochhann et al. (2016) provides a plausible age model for the Most Basin sediments. It gives a better fit than the ATNTS2012 for reversals older than 17.4 Ma (Table 1).

One of several possible criteria confirming the correct timing of the polarity reversals in sedimentary sequences is a lack of abrupt changes in the mean deposition rate at the polarity reversals (Channell et al., 2013; Ohneiser et al., 2013), where the deposition mechanisms remained unchanged and there are no (apparent) hiatuses in the record. For HK591, the combined polarity time scale and eccentricity tuned models produced only moderately fluctuating deposition rates (18-21 cm/kyr), while the Kochhann et al. (2016) polarity time scale produced a systematically upward-increasing deposition rate in HK591 (from 13 to 30 cm/kyr). In HD50, both the ATNTS2012 and Kochhann et al. (2016) time scales individually produced upward decreases in sedimentation rates, while in the combined time scale the rate was nearly constant. The only core with a mean deposition rate substantially changing is DO565 in its lowermost part, but it occurred in all examined time scales, which shows a real change and not processing artefact.

The uncertainty of the age model for the Libkovice Member in the Most Basin (ca. 16.5-17.5 Ma) can be estimated to be the order of few precession cycles at maximum. That estimate is based on the possibility to match eccentricity and precession amplitudes peak-to-peak to the K/Al or K/Ti data, supported by the resulting rather uniform sedimentation rates and the 'testPrecession' method (Zeeden et al. 2015; Fig. 7). We, however, expect larger uncertainty in the Holešice Member (before 17.5 Ma) due to locally and temporally variable uneven deposition rates and patterns that match the orbital solution in less detail.

4.2 Interpretation of geochemical patterns in the Most Basin

Clay minerals are the main constituents of the Most Basin lacustrine sediments, controlling their chemical composition. The clay composition may be controlled by at least three factors: (1) spatially variable sediment provenance, if source areas have specific clay mineralogy, (2) grain-size segregation on transport and deposition, and (3) chemical weathering intensity. Recently Wan et al. (2017) have discussed a combination of these aspects. Their deciphering in the Most Basin would require detailed knowledge of its palaeogeography and palaeolimnology, which is not available due to erosion and denudation of the original Most Basin catchment. Each of the three above listed factors may reflect climate, in particular through the amount and seasonal distribution of precipitation and the resulting river morphology and -network. The periodicity in clay mineral proportions (revealed here by K variability) in continental sedimentary records would point rather to mechanisms (2) and (3), and actually the interplay of transport and weathering seems responsible for the K/Al or K/Ti variations in the Most Basin sediments.

Practically important for the use of K-chemostratigraphy is the choice of the normalizing element. In this work we use either Al or Ti (in particular in the Osek Member). The variations in K concentrations are partly related to the grain-size changes. Interplay of K, Al, and Ti concentrations in sediments of different coarseness, provenance, and geochemical maturity (Zabel et al., 2001; Bouchez et al., 2011; von Eynatten et al., 2016; Liu et al., 2017) is individual for each catchment. In fine, repeatedly recycled, chemically mature sediments (Bouchez et al., 2011), K/Ti increases in the finest fractions while it decreases in younger, fresh, less mature sediments (von Eynatten et al., 2016). The Al content increases in the finest fractions in both cases. The K depletion by enhanced chemical weathering may either be counteracted or amplified by simultaneous change of the sediment grain size, depending on the illite contribution (this mineral retains K in the finest fraction) and major carriers of Ti (either silt-sized heavy minerals, von Eynatten et al., 2016, or the finest pedogenic anatase and clay minerals, as in laterites). The choice of the element normalizer must thus be empirical. In the Osek Member in OS17 core, the K/Al element ratio does not carry an orbital signal while K/Ti does and K/Ti shows more orbital-scale variability also in the lowermost part of DO565.

Kaolinite is a weathering products of mafic volcanic rocks under warm and humid (typically tropical) climate, while illite-smectite structures are intermediate and metastable at the time scale of 10^3 - 10^4 yr (Ryan and Huertas, 2009), i.e., sufficiently fast to preserve the imprint of the Earth's orbital cycles (e.g., Moiroud et al., 2012; Ghirardi et al., 2014).

Integrated sedimentological, geochemical, and statistical approaches document the pacing of the Earth's orbit on dissolution (or decreased primary production) of carbonates in marine environments, $\delta^{18}\text{O}$ and $\delta^{13}\text{C}$ patterns in the sediments from the Pacific and Atlantic oceans (Holbourn et al., 2014, 2015; Kochhann et al., 2016; Liebrand et al., 2016; De Vleeschouwer et al., 2017), extent of the Antarctic ice sheet (Passchier et al., 2011; Liebrand et al., 2011, 2017), water balance (Valero et

al., 2014) and sediment supply (Valero et al., 2016) in continental environments in the Oligocene and Miocene. The eccentricity is one of the dominant motives also in the Most Basin sediment geochemistry, with superimposed influence of precession as discussed above, while obliquity is transiently dominant when the eccentricity decreases (Matys Grygar et al., 2014, 2017a, 2017b), similarly as in other Miocene sediment sequences (e.g., Zeeden et al., 2013). Under relatively warm conditions of the late Burdigalian in the studied area (frost-free coldest months, mean annual temperature ~ 17 °C, Teodoridis and Kvaček 2015), the chemical weathering intensity was probably controlled by humidity (mean annual precipitation was 1000-1500 mm, Utescher et al., 2012; Teodoridis and Kvaček 2015). Consistently with the model of cooler global climate (heavier $\delta^{18}\text{O}$) under low eccentricity (De Vleeschouwer et al., 2017), we may also expect lower global sea level including water bodies relevant for the Most Basin, i.e., North Sea and Paratethys area, and lower seasonal thermal gradients between ocean surface and continents, both decreasing import of humidity to the study area, and correspondingly lower intensity of chemical weathering in the lake catchment. Such interpretation would be consistent with the deposition of sediments most depleted in K in the Most Basin during the high eccentricity periods observed in pre-MCO and early MCO intervals (Figs 1, 13, and 14).

4.3 Orbital forcing in the Most Basin record and its comparison with global records

The first comparison of the Most Basin record with benthic $\delta^{18}\text{O}$ curve has been shown in Matys Grygar et al. (2017b). Their comparison is here corroborated, the age model is discussed in more details and is better supported by magnetic polarity analysis and eccentricity tuning. Most early Miocene marine records do not pick up the precession cycles, while the Most Basin record does record precession related variability in several intervals. Detailed comparison of the Most Basin and marine records is hindered by the uncertainty of the polarity time scale to <100 kyr, as discussed in Introduction and shown in Table 1. To minimise the impact of several polarity time scales, we compared the Most Basin K/Al curve with $\delta^{18}\text{O}$ and $\delta^{13}\text{C}$ curves by Kochhann et al. (2016) in Fig. 14, currently the most detailed reference dataset openly available. In Fig. 14, we used the same polarity time scale as Kochhann et al. (2016), i.e., the differences in timing our continental K/Al record and marine isotopic record by Kochhann et al. (2016) may only be caused by intrinsic errors of their depth-age models, such as lock-in effects and stratigraphic fidelity of individual cores. The majority of prominent K/Al minima in the Most Basin deposits may be associated with the marine $\delta^{18}\text{O}$ and/or $\delta^{13}\text{C}$ minima with misfits <5 kyr (Fig. 14). Exceptions (K5 and the Lom Member) are discussed below.

Earth's climate response to individual orbital cycles, long and short eccentricities, obliquity, and climatic precession, has shown temporally variable sensitivity in the past. We observed such

variable sensitivity also in the Most Basin (Matys Grygar et al. 2014, 2017b). Since the beginning of the Most Basin record above the main coal seam, the K/Al (or K/Ti) variations show precession control (the Holešice Member), then K/Al (or K/Ti) minima are associated with eccentricity maxima (the Libkovice Member, Fig. 14). The eccentricity control in the Most Basin was strengthened after ~17.7 Ma, i.e., after the basin-wide transformation of swamps with local water bodies to a single lake. That process was coeval with the first stage of the pre-MCO Antarctic deglaciation near time of C5Dr.1n (Levy et al., 2017), as discussed in Matys Grygar et al. (2017b).

An abrupt change in the expression of eccentricity and precession in the studied time interval was found near the K5 minimum. The sediments younger than K5 (P1 interval, 16.95 to 16.70 Ma, Fig. 13) responded to precession to the level of straightforward consecutive association of each K/Al minimum to an individual precession cycle (Fig. 13). The sediments of the P1 interval were deposited in the persistently high-eccentricity interval between 16.95 and 16.7 Ma of the astronomical solution (Laskar et al., 2004). The break near K5 (17.05 Ma) is – within uncertainty of dating – coeval with the major pre-MCO shift in $\delta^{13}\text{C}$ and $\delta^{18}\text{O}$ (start of the MCO) dated to ~17.0 Ma by Holbourn et al. (2015) and Kochhann et al. (2016; Fig. 14) and 17.2 Ma by Miller et al. (2017). In that period of time Kochhann et al. (2016) found the strongest carbonate dissolution in their record, similarly as further researchers (see Introduction). In the P1 interval of HK591 core, the total sulphur increased from 0.09 to 0.21 %, total organic carbon increases from 2.0 to 2.9 %, and previously presented trace fossils *Planolites montanus*, small burrows of unknown invertebrates (Mikuláš et al., 2003) were replaced by occasional *Trichichnus*, bacterially produced “pyrite wires”, all showing a less oxygenated lake bottom.

The orbital signature in the Most Basin almost vanished after 16.6-16.7 Ma, i.e., after the partial recovery of a negative shift in marine $\delta^{13}\text{C}$ (Fig. 14). A first prominent $\delta^{13}\text{C}$ maximum in the global carbon isotopic data was found at ~16.6 Ma (Holbourn et al., 2015, Kochhann et al., 2016) and 16.8 Ma by Miller et al. (2017). That difference in dating represents real uncertainty of marine sedimentary archives in that particular period of time described in the introduction. The subsequent weak sensitivity of the Most Basin continental deposits to orbital parameters is, in our opinion, something to be expected under stable warm climatic mode of the MCO.

The Lom Member (~ 16.4 Ma) with chemically remarkably mature sediments (K/Al minimum in fine sediment dominated by kaolinite according to high Al/Si, Fig. 11) was deposited between two high eccentricity maxima (Fig. 13). The overlying sediments (the Osek Member, younger than ~16.35 Ma) only show weak orbital signatures except for a triplet of grain-size controlled “fingers” in the interval labelled P2 (Figs 6D and 12).

4.4 Other possible controls in the Most Basin sedimentary record

Autocyclicity (intrinsic or endogenic control) may be a major driving force in lithological and geochemical records in continental basins, particularly in sediment sequences of laterally unstable river systems (Hajek et al. 2012; discussion in Abels et al., 2013). In an autocyclic fluvial succession, Hajek et al. (2012) found lateral and vertical lithological (facies) variability with no qualitative vertical variations (i.e., no temporal development) in individual fluvial facies. *Vice versa*, in a climate- and orbitally-controlled fluvial succession, Abels et al. (2012) and Kraus et al. (2015) found laterally stable strata with specific qualitative features ($\delta^{13}\text{C}$ shift) and cyclic vertical evolution of lithology of the same facies. In the Most Basin, sediments above the main coal seam, in particular the Libkovice Member, show vertical facies stability with laterally stable geochemical features showing regular vertical cyclicity. Most importantly, we demonstrated the typical hierarchical pattern of precession amplitude matching eccentricity signals, consistent with established magnetostratigraphy. These facts prove that the Most Basin fill was not dominantly shaped by autocyclic fluvial processes, but that orbital forcing played a major role.

In the age model based exclusively on magnetic polarity (according to ATNTS2012 in this time interval), the K5 minimum in the Most Basin record is dated to 17.05 Ma. Results from the eccentricity-matched age model is compatible with such a date, with K5 coeval with a minor precession maximum. In contrast to the preceding major K minima K2 to K4, K5 does match neither the earliest eccentricity maximum (17.093 Ma, see misfit in 'testPrecession' in Figs 10C and 10D) nor marine $\delta^{18}\text{O}$ minimum (Fig. 14). The K5 minimum could thus be attributed to a specific local or regional factor, probably an environmental extreme, which would deserve further examination due to its position close to the MCO onset.

The period of elevated precession power in the Most Basin record (P1 interval, Figs 6B, 13, and 14) was terminated at 16.65 Ma. Recently Sant et al. (2017a) attributed the shift of the brackish to freshwater and continental environment in the North Alpine Foreland Basin (NAFB) between 16.7 and 16.4 Ma to tectonic movements. We might speculate that the Most Basin as a part of the same rift system (European Cenozoic Rift System) might also respond to the same forcing. Indeed, geologists observed signs of novel direction of clastic input into the Most Basin during the deposition of Lom and Osek members that could reflect a tectonic change and a shift in source material. However, the mineralogy and geochemistry in the Libkovice and Osek members remained more or less the same as in the preceding Libkovice Member. Moreover, the geochemical mechanism behind the K/Al environmental proxy is general and we suppose it should not be sensitive to the actual palaeogeography. Thus, if the Lom Member formation was related to a tectonic change, it might have shown a central European scale.

In the introduction, we mentioned the hypothesis that the MCO was triggered by the Columbia River Basalt Group (Courtilot et al., 2003). The dating of the Columbia River basalt floods has recently attracted systematic attention of several researchers (Barry et al., 2010; Baksi 2012; Mahood

and Benson, 2017), which resulted in refined age constraints for the CRBG phases. The major part of the basalts of the CRBG was effused around 16.0 Ma, while the volcanism started at ~16.6 Ma (Barry et al., 2010; Mahood and Benson, 2017), coevally with the first $\delta^{13}\text{C}$ maximum of the Monterey excursion (Fig. 14; see also Fig. 9 in Mahood and Benson, 2017). This episode coincided with the boundary the Libkovice/Lom members, and the vanishing of orbital signal in the Most Basin (Fig 13 and 14). The onset of the Lom Member thus may indicate relevant, non-orbitally triggered environmental change in the Most Basin, perhaps coeval with environmental changes elsewhere in the Earth.

5 Conclusions

The Most Basin record was extended by two cores and some discrepancies from original studies were removed. The Most Basin record now starts at subchron C5Dr.1n, due to a refinement of the depth-age model for HK591 and HD50 cores, where we solved previous ambiguity in the identification of orbital signatures. Due to new established magnetic polarity analysis from the OS17 core, the record now ends at C5Dn.1n chron in the uppermost part of the Burdigalian. This work highlights the performance of the normalised K concentration as a proxy for continental weathering and palaeoclimate on orbital time scales. The variations in K concentrations are not controlled exclusively by grain-size changes (Al/Si and Zr/Rb variations), although in some cases those parameters vary in interplay. The K/Al or K/Ti minima are interpreted as maxima of chemical weathering intensity in the catchment; these coincided with periods of high eccentricity and low $\delta^{18}\text{O}$ in marine stable isotope data. We conclude that the normalised K concentrations are worthy testing as a perspective continental weathering and climate proxy for siliciclastic sediments, assuming the actual normalisation corrects for grain-size effects. The major environmental events in the Most Basin sedimentation above the main coal seam can be related to the major global changes of the period preceding the Miocene climatic optimum. Two important environmental changes in the Most Basin, apparently not resulting from orbital forcing, occurred at ca. 17.05 Ma (K5 minimum) and around 16.6 Ma (16.65 Ma, vanishing of orbital signatures in the Libkovice Member and 16.5 Ma, boundary of the Libkovice/Lom members). Because relevant environmental changes in both time intervals occurred also elsewhere, they may indicate yet unrecognised or poorly understood environmental disruptions which triggered and shaped the MCO.

Acknowledgments

This work would not be possible without the access to drill cores HD50 and OS17 provided generously by the VODAMIN project coordinated by Palivový Kombinát Ústí, s.p. Drill cores HJK772, HK591, and DO565 were kindly provided by North Bohemian Mines in Bílina. The

laboratory work and data processing were performed under support from the Czech Science Foundation (project number 16-00800S). The research is a part of research plan of the Institute of Inorganic Chemistry in Řež funded by the Czech Academy of Sciences.

TMG was responsible for XRF data interpretation and prepared manuscript drafts, KM provided the geological background, supervised drill coring, and conducted field examination of the drill cores, PS and his team was responsible for magnetic polarity analyses. MM performed spectral analysis and contributed to data presentation, CZ applied the ‘testPrecession’ and contributed to data presentation. The authors thank to M. Faměra, M. Maříková, and P. Vorm (Institute of Inorganic Chemistry in Řež) for drill core sampling, sample processing, and analysis (XRF and CEC), and K. Čížková and Š. Kdýr (Geological Institute in Prague) for assistance with sampling, analysis, and interpretation of magnetic polarities.

The authors thanks to two anonymous reviewers, whose careful, critical, and constructive reports considerably improved this manuscript.

References

- Abels H. A., Abdul Aziz H., Krijgsman W., Smeets S. J. B., Hilgen F. J., 2010. Long-period eccentricity control on sedimentary sequences in the continental Madrid Basin (middle Miocene, Spain). *Earth Planet. Sci. Lett.* 289, 220–231.
- Abels, H. A., Kraus, M. J. Gingerich Philip D., 2013. Precession-scale cyclicity in the fluvial lower Eocene Willwood Formation of the Bighorn Basin, Wyoming (USA). *Sedimentology* 60, 1467–1483.
- Armstrong M^cKay D. I., Tyrrell T., Wilson P. A., Foster G. L., 2014. Estimating the impact of the cryptic degassing of Large Igneous Provinces: A mid-Miocene case-study. *Earth Planet. Sci. Letters Lett.* 403, 254–262.
- Baksi A. K., 2012. “New ⁴⁰Ar/³⁹Ar dating of the Grande Ronde lavas, Columbia River Basalts, USA: Implications for duration of flood basalt eruption episodes” by Barry et al. (2010) – Discussion. *Lithos* 146–147, 293–299.
- Barry T. L., Self, S., Kelley, S. P., Reidel S., Hooper P., Widdowson M., 2010. New ⁴⁰Ar/³⁹Ar dating of the Grande Ronde lavas, Columbia River Basalts, USA: Implications for duration of flood basalt eruption episodes. *Lithos* 118, 213-222.
- Billups, K., Pälike H., Channell J. E. T., Zachos J. C., Shackleton N. J., 2004. Astronomic calibration of the late Oligocene through early Miocene geomagnetic polarity time scale. *Earth Planet. Sci. Lett.* 224, 33–44.
- Böhme M., 2003. The Miocene Climatic Optimum: evidence from ectothermic vertebrates of Central Europe. *Palaeogeogr. Palaeoclimatol. Palaeoecol.* 195, 389-401.

- Bouchez, J., Gaillardet, J., France-Lanord, C., Maurice, L., Dutra-Maia, P., 2011. Grain size control of river suspended sediment geochemistry: clues from Amazon River depth profiles. *Geochem. Geophys. Geosyst.* 12, Q03008.
- Channell J. E. T., Ohneiser C., Yamamoto Y., Kesler M. S., 2013. Oligocene-Miocene magnetic stratigraphy carried by biogenic magnetite at sites U1334 and U1335 (equatorial Pacific Ocean). *Geochem. Geophys. Geosyst.* 14, 265–282.
- Chen, J., Chen, Y., Liu, L.-W., Ji, J.-F., Balsam, W., Sun, Y.-B., Lu, H.-Y., 2006. Zr/Rb ratio in the Chinese loess sequences and its implication for changes in the East Asian winter monsoon strength. *Geochim. Cosmochim. Acta* 70, 1471-1482
- Clift P. D., Wan S.-M., Blusztajn J., 2014. Reconstructing chemical weathering, physical erosion and monsoon intensity since 25 Ma in the northern South China Sea: A review of competing proxies. *Earth-Sci. Rev.* 130, 86–102.
- Courtillot, V. E., Renne, P. R., 2003. On the ages of flood basalt events. *C. R. Geosci.* 335, 113–140.
- De Vleeschouwer D., Vahlenkamp M., Crucifix M., Pälike H., 2017. Alternating Southern and Northern Hemisphere climate response to astronomical forcing during the past 35 m.y. *Geology*, 45, 375–378.
- Dill, H.G., 2001. The geology of aluminium phosphates and sulphates of the alunite group minerals: a review. *Earth Sci. Rev.* 53, 35-93.
- Elznic, A., Čadková, Z., Dušek, P., 1998. Paleogeografie terciérních sedimentů severočeské pánve (Paleogeography of Tertiary sediments of the North Bohemian Basin). *Sborník geologických věd, Geologie* 48, 19-46.
- Fejfar, O., Kvaček, Z., 1993. Excursion nr. 3, Tertiary basins in Northwest Bohemia. – 63. *Jahrestagung der Paläontologischen Gesellschaft: 1-35; Prague.*
- Gasson E, DeConto R.M., Pollard D, Levy R.H., 2016), Dynamic Antarctic ice sheet during the early to mid-Miocene. *Proc. Nat. Acad. Sci. USA* 113, 3459–3464.
- Ghirardi, J., Deconinck, J.-F., Pellenard, P., Martinez, M., Bruneau, L., Amiotte-Suchet, P., Pucéat, E., 2014. Multi-proxy orbital chronology in the aftermath of the Aptian Oceanic Anoxic Event 1a: Palaeoceanographic implications (Serre Chaitieu section, Vocontian Basin, SE France). *Newslett. Stratigraphy* 47, 247–262.
- Grygar, T., Kadlec, J., Žigová, A., Mihaljevič, M., Nekutová, T., Lojka, R., Světlík, I. 2009. Chemostratigraphic correlation of sediments containing expandable clay minerals based on ion exchange with Cu(II) complex with triethylenetetramine. *Clays Clay Miner.* 57, 168–182.
- Hajek, E.A., Heller, P.L., Schur, E.L., 2012. Field test of autogenic control on alluvial stratigraphy (Ferris Formation, Upper Cretaceous–Paleogene, Wyoming). *GSA Bulletin* 124; 1898–1912.

- Havelcová, M., Sýkorová, I., Mach, K., Trejtnarová, H., Blažek, J., 2015. Petrology and organic geochemistry of the lower Miocene lacustrine sediments (Most Basin, Eger Graben, Czech Republic). *Internat. J. Coal Geol.* 139, 26–39.
- Hilgen, F. J., Lourens, L. J., Van Dam, J. A., 2012. The Neogene Period. In: Gradstein, F. M., Ogg, J. G., Schmitz, M. D., Ogg, G. M., *The Geologic Time Scale 2012*. Amsterdam, Elsevier BV.
- Holbourn, A., Kuhnt, W., Lyle, M., Schneider, L., Romero, O., Andersen, N., 2014. Middle Miocene climate cooling linked to intensification of eastern equatorial Pacific upwelling. *Geology* 42, 19–22.
- Holbourn, A., Kuhnt, W., Kochhann, K. G. D., Andersen N., Meier K.J. S., 2015. Global perturbation of the carbon cycle at the onset of the Miocene Climatic Optimum. *Geology* 43, 123–126.
- Kamikuri, S.-I., Moore, T. C., 2017. Reconstruction of oceanic circulation patterns in the tropical Pacific across the early/middle Miocene boundary as inferred from radiolarian assemblages. *Palaeogeogr. Palaeoclimatol. Palaeoecol.* 487, 136–148.
- Kirschvink, J. L., 1980. The least-squares line and plane and the analysis of palaeomagnetic data. *Geophys. J. Royal Astronomical Soc.* 62, 699–718.
- Kochhann, K. G. D., Holbourn, A., Kuhnt, W., Channell, J. E. T., Lyle, M., Shackford, J. K., Wilkens, R. H., Andersen, N., 2016. Eccentricity pacing of eastern equatorial Pacific carbonate dissolution cycles during the Miocene Climatic Optimum, *Paleoceanogr.* 31, 1176–1192.
- Kotthoff, U., Greenwood, D. R., McCarthy, F. M. G., Muller-Navarra, K., Prader, S., Hesselbo, S. P., 2014. Late Eocene to middle Miocene (33 to 13 million years ago) vegetation and climate development on the North American Atlantic Coastal Plain (IODP Expedition 313, Site M0027). *Clim. Past* 10, 1523–1539.
- Kraus, M.J., Woody, D. T., Smith, J. J., Dukic, V., 2015. Alluvial response to the Paleocene–Eocene Thermal Maximum climatic event, Polecat Bench, Wyoming (U.S.A.). *Palaeogeogr. Palaeoclimatol. Palaeoecol.* 435, 177–192.
- Kvaček Z, Böhme M, Dvořák Z, Mach K, Prokop J, Rajchl M, 2004. Early Miocene freshwater and swamp ecosystems of the Most Basin (northern Bohemia) with particular reference to the Bílina Mine section. *J. Czech Geol. Soc.* 49, 1–39.
- Laskar, J., Robutel, P., Joutel, F., Gastineau, M., Correia, A. C. M., Levrard, B., 2004. A long-term numerical solution for the insolation quantities of the Earth. *Astronomy Astrophys.* 428, 261–285.
- Levy R. et al., 2016. Antarctic ice sheet sensitivity to atmospheric CO₂ variations in the early to mid-Miocene. *Proc. Nat. Acad. Sci. USA* 113, 3453–3458.
- Liebrand, D., Lourens, L. J., Hodell, D. A., de Boer, B., van de Wal, R. S. W., Palike, H., 2011. Antarctic ice sheet and oceanographic response to eccentricity forcing during the early Miocene, *Clim. Past* 7, 869–880.

- Liebrand D. et al., 2016. Cyclostratigraphy and eccentricity tuning of the early Oligocene through early Miocene (30.1–17.1 Ma): *Cibicides mundulus* stable oxygen and carbon isotope records from Walvis Ridge Site 1264. *Earth Planet. Sci. Lett.* 450, 392–405
- Liebrand D. et al., 2017. Evolution of the early Antarctic ice ages. *Proc. National Acad. Sci.* 114, 3867–3872
- Liu X-T, Rendle-Bühning R, Henrich R (2017) Geochemical composition of Tanzanian shelf sediments indicates Holocene climatic and sea-level changes. *Quaternary Research* 87, 442–454.
- Mach, K., Teodoridis, V., Matys Grygar, T., Kvaček, Z. Suhr, P. & Standke, G., 2014. An evaluation of paleogeography and paleoecology in the Most Basin (Czech Republic) and Saxony (Germany) from the late Oligocene to the early Miocene. *N. Jb. Geol. Paläontol. Abh.* 272/1, 13–45.
- Mahood G. M., Benson T. R., 2017. Using $^{40}\text{Ar}/^{39}\text{Ar}$ ages of intercalated silicic tuffs to date flood basalts: Precise ages for Steens Basalt Member of the Columbia River Basalt Group. *Earth Planet. Sci. Lett.* 459, 340–351.
- Matys Grygar, T., Mach, K., 2013. Regional chemostratigraphic key horizons in the macrofossil-barren siliciclastic lower Miocene lacustrine sediments (Most Basin, Eger Graben, Czech Republic), *Bull. Geosci.* 88, 557–571.
- Matys Grygar, T., Mach, K., Pruner, P., Schnabl, P., Laurin, J., Martinez, M., 2014. A lacustrine record of the early stage of the Miocene Climatic Optimum in Central Europe from the Most Basin, Ohře (Eger) Graben, Czech Republic, *Geol. Mag.* 151, 1013-1033.
- Matys Grygar, T., Mach, K., Hošek, M., Schnabl, P., Martinez, M., Koubová, M., 2017a. Early stages of clastic deposition in the Most Basin (Ohře Rift, Czech Republic, Early Miocene): timing and possible controls. *Bull. Geosci.* 92, 337–355.
- Matys Grygar, T., Hošek, M., Mach, K., Schnabl, P., Martinez, M., 2017b. Climatic instability before the Miocene Climatic Optimum reflected in a Central European lacustrine record from the Most Basin in the Czech Republic. *Palaeogeogr. Palaeoclimatol. Palaeoecol.* 485, 930–945.
- Marshall, N., Zeeden, C., Hilgen, F., Krijgsman W., 2017. Milankovitch cycles in an equatorial delta from the Miocene of Borneo. *Earth Planet. Sci. Lett.* 472, 229–240.
- Meier, L. P., Kahr, G., 1999. Determination of the cation exchange capacity (CEC) of clay minerals using the complexes of copper(II) ion with triethylenetetramine and tetraethylenepentamine, *Clays Clay Miner.* 47, 386–388.
- Mikuláš, R., Mach, K., Dvořák, Z., 2003. Bioturbation of claystones of the Most Basin in the Bílina quarry (Miocene, Czech Republic). *Acta Universitatis Carolinae, Geologica* 47, 79-85.
- Miller, K. G., Baluyot, R., Wright, J. D., Kopp, R. E., Browning, J. V., 2017. Closing an early Miocene astronomical gap with Southern Ocean O-18 and C-13 records: Implications for sea level change. *Paleoceanography* 32, 600–621.

- Moiroud, M., Martinez, M., Deconinck, J.-F., Monna, F., Pellenard, P., Riquier, L., Company, M., 2012. High-resolution clay mineralogy as a proxy for orbital tuning: Example of the Hauterivian–Barremian transition in the Betic Cordillera (SE Spain). *Sedim. Geol.* 282, 336–346.
- Molliex, S., Jouet, G., Freslon, N., Bourlès, D. L., Authemayou, C., Moreau, J., Rabineau M., 2017. Controls on Holocene denudation rates in mountainous environments under Mediterranean climate. *Earth Surf. Process. Landforms* 42, 272–289.
- Novák, F., Pekárková, R., Ševců, J., 1993. Barium rich crandallite from the Nástup Tušimice quarry (North-Bohemian Brown-Coal Basin). *Věst. Čs. Geol. Úst.* 68, 53–57.
- Ohneiser, C., Acton, G., Channell, J. E. T., Wilson, G. S., Yamamoto, Y., Yamazaki, T., 2013. A middle Miocene relative paleointensity record from the Equatorial Pacific. *Earth Planet. Sci. Lett.* 374, 227–238.
- Pälike H. et al., 2012. A Cenozoic record of the equatorial Pacific carbonate compensation depth. *Nature* 488, 609–615.
- Passchier, S., Browne, G., Field, B., Fielding, C.R., Krissek, L.A., Panter, K., Pekar, S.F., 2011. Early and middle Miocene Antarctic glacial history from the sedimentary facies distribution in the AND-2A drill hole, Ross Sea, Antarctica. *Geol. Soc. Am. Bull.* 123, 2352–2365.
- Phillips, D., Matchan, E. L., 2013. Ultra-high precision $^{40}\text{Ar}/^{39}\text{Ar}$ ages for Fish Canyon Tuff and Alder Creek Rhyolite sanidine: New dating standards required? *Geochim. Cosmochim. Acta* 121, 229–239.
- Pippèrr, M., Reichenbacher, B., 2017. Late Early Miocene palaeoenvironmental changes in the North Alpine Foreland Basin. *Palaeogeogr. Palaeoclimatol. Palaeoecol.* 468, 485–502.
- R Core Team, 2017. R: A Language and Environment for Statistical Computing. <https://www.R-project.org/>.
- Rajchl, M., Uličný, D., Grygar, R., Mach, K., 2009. Evolution of basin architecture in an incipient continental rift: the Cenozoic Most Basin, Eger Graben (Central Europe). *Basin Res.* 21, 269–294.
- Reichenbacher, B., Krijgsman, W., Lataster, Y., Pippèrr, M., Van Baak, C. G. C., Chang, L., Kalin, D., Jost, J., Doppler, G., Jung, D., Prieto, J., Aziz, H. A., Bohme, M., Garnish, J., Kirscher, U., Bachtadse, V., 2013. A new magnetostratigraphic framework for the Lower Miocene (Burdigalian/Ottangian, Karpatian) in the North Alpine Foreland Basin. *Swiss J. Geosci.* 106, 309–334.
- Ryan, P.C., Huertas, F.J., 2009. The temporal evolution of pedogenic Fe–smectite to Fe–kaolin via interstratified kaolin–smectite in a moist tropical soil chronosequence. *Geoderma* 151, 1–15.
- Sant, K., Kirscher, U., Reichenbacher, B., Pippèrr, M., Jung, D., Doppler, G., Krijgsman, W., 2017a. Late Burdigalian sea retreat from the North Alpine Foreland Basin: new magnetostratigraphic age constraints. *Global Planet. Change* 152, 38–50.

- Sant, K., Palcu, D. V., Mandic, O., Krijgsman, W., 2017b. Changing seas in the Early–Middle Miocene of Central Europe: a Mediterranean approach to Paratethyan stratigraphy. *Terra Nova* DOI: 10.1111/ter.12273.
- Teodoridis, V., Kvaček, Z. 2015. Palaeoenvironmental evaluation of Cainozoic plant assemblages from the Bohemian Massif (Czech Republic) and adjacent Germany. *Bull. Geosci.* 90, 695–720.
- Tian, J., Zhao, Q.-H., Wang, P.-X., Li, Q.-Y., Cheng, X.-R., 2008. Astronomically modulated Neogene sediment records from the South China Sea. *Paleoceanogr.* 23, PA3210.
- Turco, E., Hüsing, S., Hilgen, F., Cascella, A., Gennari, R., Iaccarino, S. M., Sagnotti, L., 2017. Astronomical tuning of the La Vedova section between 16.3 and 15.0 Ma. Implications for the origin of megabeds and the Langhian GSSP. *Newslett. Stratigr.* 50, 1–29.
- Uličný, D., Jarvis, I., Grocke, DR., Čech, S., Laurin, J., Olde, K., Trabucho-Alexandre, J., Švábenická, L., Pedentchouk, N., 2014. A high-resolution carbon-isotope record of the Turonian stage correlated to a siliciclastic basin fill: Implications for mid-Cretaceous sea-level. *Palaeogeogr. Palaeoclimatol. Palaeoecol.* 405, 42–58.
- Utescher, T., Ashraf, A.R., Dreist, A., Dybkjær, K., Mosbrugger, V., Pross, J., Wilde, V., 2012. Variability of Neogene continental climates in Northwest Europe – a detailed study based on microfloras. *Turkish J. Earth Sci.* 21, 289–314.
- Valero L., Garcés M., Cabrera L., Costa E., Sáez A., 2014. 20 Myr of eccentricity paced lacustrine cycles in the Cenozoic Ebro Basin. *Earth Planet. Sci. Lett.* 408, 183-193.
- Valero L., Cabrera, L., Saez, A., Garcés, M., 2016. Long-period astronomically-forced terrestrial carbon sinks. *Earth Planet. Sci. Lett.* 444, 131-138
- Valero L., Huerta P., Garcés M., Armenteros I., Beamud E., Gómez-Paccard M., 2017. Linking sedimentation rates and large-scale architecture for facies prediction in nonmarine basins (Paleogene, Almazán Basin, Spain). *Basin Research* 29 (S1), 213–232.
- von Eynatten, H., Tolosana-Delgado, R., Karius, V., Bachmann, K., Caracciolo, L., 2016. Sediment generation in humid Mediterranean setting: Grain-size and source-rock control on sediment geochemistry and mineralogy (Sila Massif, Calabria). *Sedim. Geol.* 336, 68–80.
- Wan, S. M., Clift, P. D., Zhao, D. B., Hovius, N., Munhoven, G., France-Lanord, C., Wang, Y.-X., Xiong, Z.-F., Huang, J., Yu, Z.-J., Zhang, J., Ma, W.-T., Zhang, G.-L., Li, A.-C., Li, T.-G., 2017. Enhanced silicate weathering of tropical shelf sediments exposed during glacial lowstands: A sink for atmospheric CO₂. *Geochim. Cosmochim. Acta* 200, 123–144.
- Wu, H.-C., Zhao, X.-X., Shi, M.-N., Zhang, S.-H., Li, H.-Y., Yang, T.-S., 2014. A 23 Myr magnetostratigraphic time framework for Site 1148, ODP Leg 184 in South China Sea and its geological implications. *Marine Petroleum Geol.* 58, 749–759.
- Xu, W., Ruchl, M., Jenkyns, H. C., Leng, M. J., Huggett, J. M., Minisini, D., Ullmann, C. V., Diding, J. B., Weijers, J. W. H., Storm, M. S., Percival, L. M. E., Tosca, N. J., Idiz, E. F., Tegelaar, E. W.,

- Hasselbo, S. P., 2018. Evolution of the Toarcian (Early Jurassic) carbon-cycle and global climatic controls on local sedimentary processes (Cardigan Bay Basin, UK). *Earth Planet. Sci. Lett.* 484, 396–411.
- Zabel, M., Schneider, R. R., Wagner, T., Adegbe, A. T., de Vries, U., Kolonic, S., 2001. Late Quaternary Climate Changes in Central Africa as Inferred from Terrigenous Input to the Niger Fan. *Quatern. Res.* 56, 207–217.
- Zachos, J., Pagani, M., Sloan, L., Thomas, E., Billups, K., 2001. Trends, rhythms, and aberrations in global climate 65 Ma to present. *Science* 292, 686–693.
- Zeeden, C., Hilgen, F., Westerhold, T., Lourens, L., Röhl, U., Bickert, T., 2013. Revised Miocene splice, astronomical tuning and calcareous plankton biochronology of ODP Site 926 between 5 and 14.4 Ma. *Palaeogeogr. Palaeoclimatol. Palaeoecol.* 369, 430–451.
- Zeeden, C., Hilgen, F., Hüsing, S., Lourens, L., 2014. The Miocene astronomical time scale 9–12 Ma: New constraints on tidal dissipation and their implications for paleoclimatic investigations. *Paleoceanogr. Paleoclimatol.* 29, 296–307.
- Zeeden, C., Meyers S. R., Lourens L. J., Hilgen F. J., 2015. Testing astronomically tuned age models, *Paleoceanography* 30, 369–383.

Table 1. Dating of magnetic polarity reversals (in Ma).

Onset of chron	ATNTS2012 (Hilgen et al., 2012)	U1336 (Kochhann et al. 2016)	Combined polarity time scale ¹	HD50 K/Al ²	DO565 K/Ti ²	HK591 K/Ti ²
C5Cn.3n	16.721	16.637	16.721			16.72
C5Cr	17.235	17.154	17.235	17.23		17.24
C5Dn	17.533	17.466	17.466	17.47	17.48	17.48
C5Dr.1r	17.717	17.634	17.634	17.66	17.70	17.68
C5Dr.1n	17.740	17.676				

¹ Combination of reversal dating in ATNTS2012 and Kochhann et al. (2016), ² Timing obtained by eccentricity matching of K/Al or K/Ti

Table 2. Basis for construction of depth-age models for individual cores.

Drill core ¹	Stratigraphic unit	Basis for the age models ²
OS17	Osek Mb.	Centre of C5Cn.1r (ATNTS2012) and v_{SED} ¹
	Lom Mb.	Magnetic polarity (ATNTS2012) (extrapolation from HK772)
HK772	Libkovice Mb.	Magnetic polarity (ATNTS2012)
HK591	Libkovice Mb.	Magnetic polarity (ATNTS2012)
	Holešice Mb.	Magnetic polarity (Kochhann et al., 2016)
DO565	Libkovice Mb.	Extrapolation from HK591 in the Libkovice Mb.
	Holešice Mb.	Magnetic polarity (Kochhann et al., 2016)
HD50	Libkovice Mb.	Magnetic polarity (ATNTS2012)
	Holešice Mb.	Magnetic polarity (Kochhann et al., 2016)

¹ Cores and members in cores are ordered in upward decreasing age. ² ATNTS2012 by Hilgen et al. (2012). ³ Mean sedimentation rate after compaction calculated from cyclostratigraphic analysis.

Fig. 1. Map of the Most Basin with position of drill cores discussed in this paper.

Fig. 2. The K/Ti profile in HK591 core with depth-age model based on magnetic polarity analysis (Matys Grygar et al., 2014, 2017b) and ATNTS2012 (Hilgen et al., 2012). Short eccentricity was taken from Laskar et al. (2004). Mean sedimentation rate was calculated from polarity chrons. Marks “x” and “?” indicate lack of correlation and uncertain correlation, respectively, between K/Ti minima and eccentricity maxima.

Fig. 3. Local stratigraphy of the Most Basin (adopted from Matys Grygar et al., 2017a, 2017b) with major chemostratigraphic markers used in this work.

Fig. 4. Geochemical depth profiles, magnetic polarity records, and lateral stratigraphic correlation of drill cores studied in this work.

Fig. 5. Stack of magnetic polarity records compared with ATNTS2012 (Hilgen et al., 2012) and polarity time scale by Kochhann et al. (2016). Magnetozones were considered uncertain in intervals with uncertain polarities and inappropriate lithology (coaly or sandy/silty strata).

Fig. 6. Geochemical and grain size control over K minima in individual strata for HK591 core (A and B), HD50 core (C) and OS17 core (D). K/Al minima are associated with variations of Al/Si (coarseness, clay mineral and kaolinite content), Zr/Rb (coarseness), and/or cation exchange capacity as ΔCu (content of smectite structures). Thin black arrows in logs of element ratios show geochemical trends in K minima highlighted by grey rectangles. Legend related to stratigraphic markers is in Fig. 3.

Fig. 7. Tested depth-age models (A to D) and ‘testPrecession’ graphical output (E) for K/Al in HD50 core using depth-age model shown in panel D. In panel C, eccentricity matching used for construction of panel D is shown by broad red lines. In panel D matching of prominent precession cycles is shown by orange lines.

Fig. 8. Spectral analysis of K/Ti in DO565 drill core.

Fig. 9. Depth-age model for DO565 based on eccentricity-tuning of K/Al (A) and corresponding ‘testPrecession’ graphical output (B).

Fig. 10. Revised magnetic polarity interpretation (A), eccentricity-tuned age model for K/Ti (B), and ‘testPrecession’ graphical output for K/Ti (C) and K/Al ratios (D) in HK591 drill core. In panel A,

option 1 was used previously, option 2 was used in this work. Note variable x scales in individual panels.

Fig. 11. Spectral analysis of K/Ti in OS17 drill core.

Fig. 12. Geochemical patterns and magnetic polarity in OS17 core. Chron C5Cn.2r was not recorded, as it was deposited in the Lom Member with coaly clays and coal strata.

Fig. 13. K/Al composite for the Most Basin. Dating for individual cores was constructed as described in Table 3, in cores HK and HD with minimal matching of main K minima to eccentricity maxima. Corresponding mean deposition rates between tie points are shown in top. Orbital eccentricity and climatic precession from Laskar et al. (2004) are shown in bottom.

Fig. 14. Comparison of the Most Basin composite of K/Al with marine stable isotope maps of $\delta^{13}\text{C}$ and $\delta^{18}\text{O}$ in the equatorial Pacific Ocean by Kochhann et al. (2016). Polarity time scales were taken from Kochhann et al. (2016), i.e., the Most Basin record has different dating than in Fig. 13.

Research highlights

- Continental climate record of the pre-MCO period
- Sediment record to solve uncertainty in marine archives around 17.0 Ma
- Variable environment sensitivity to orbital forcing
- Adjusted polarity timescale for the period around 17.0 Ma

ACCEPTED MANUSCRIPT

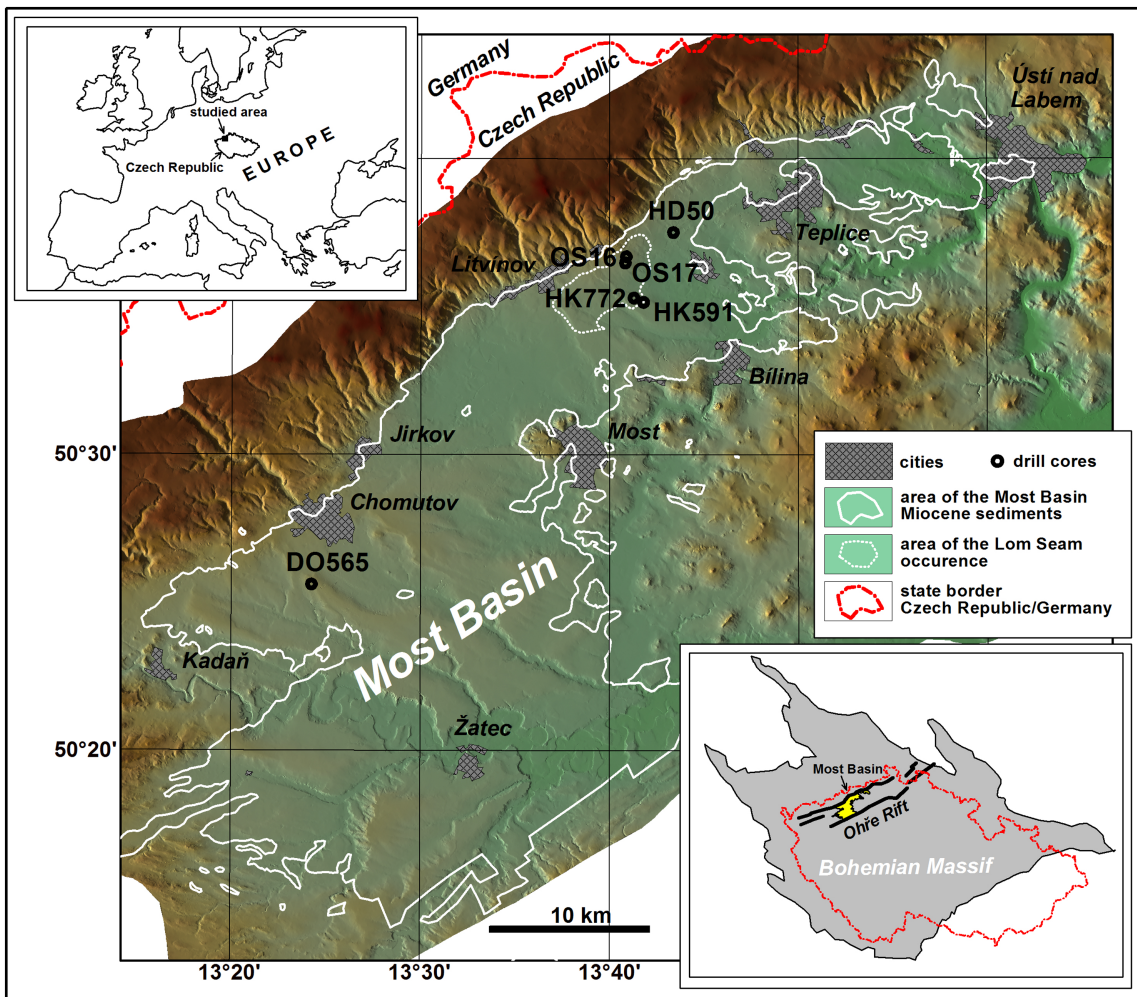


Figure 1

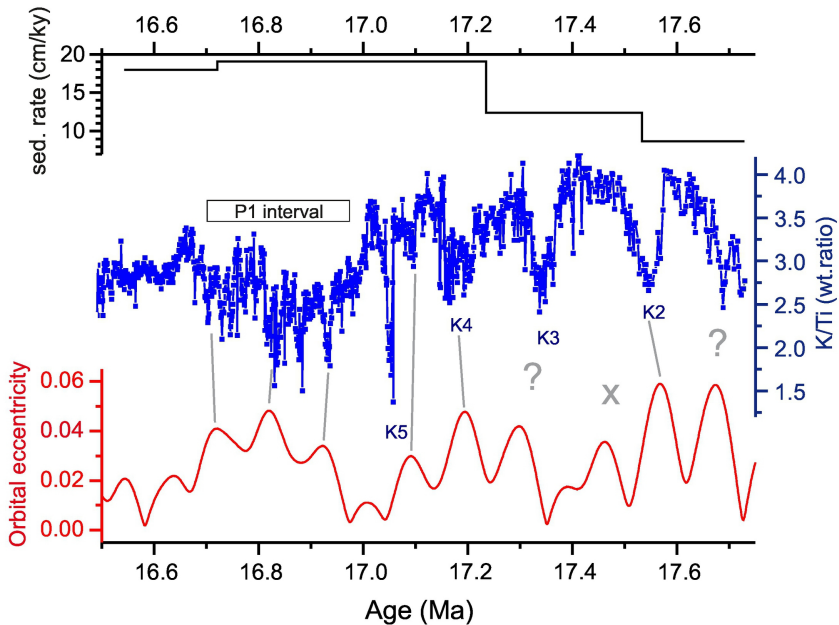


Figure 2

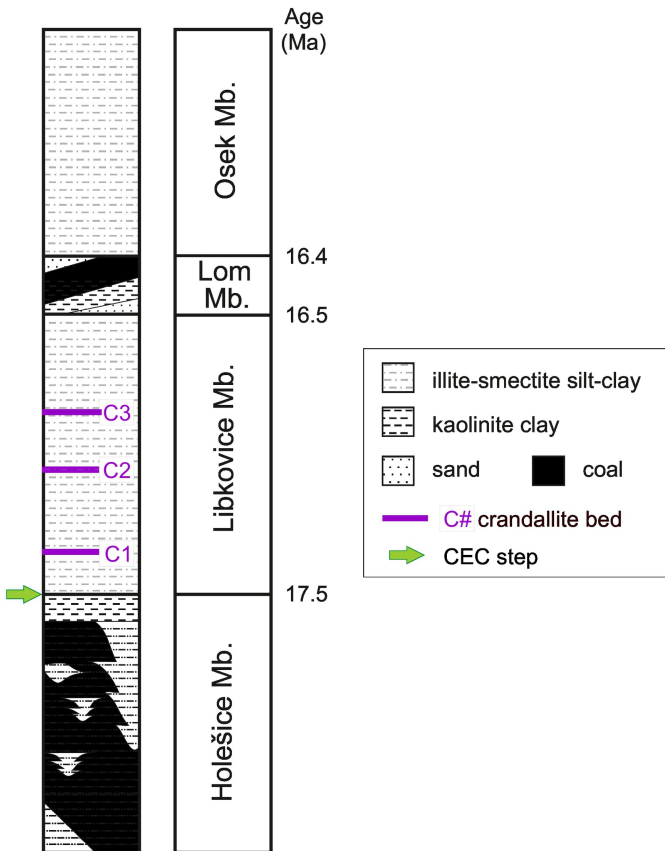


Figure 3

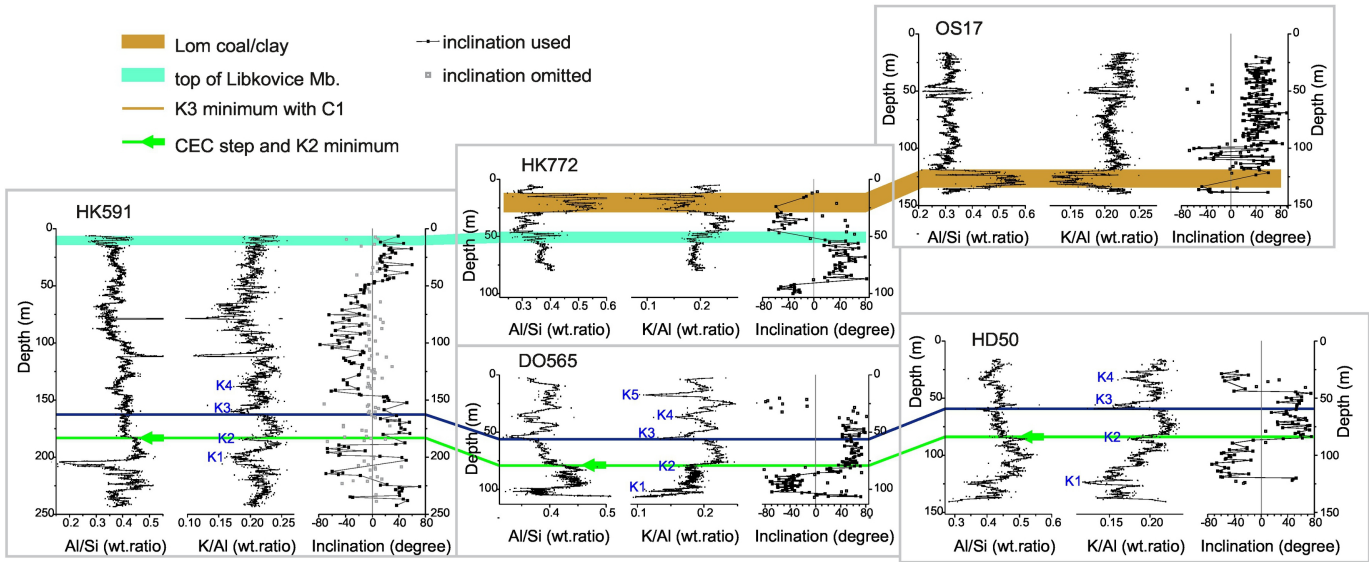


Figure 4

Inclination results:
 ■ used □ rejected

Magnetozones:
 ■ normal □ inverse
 ▒ uncertain

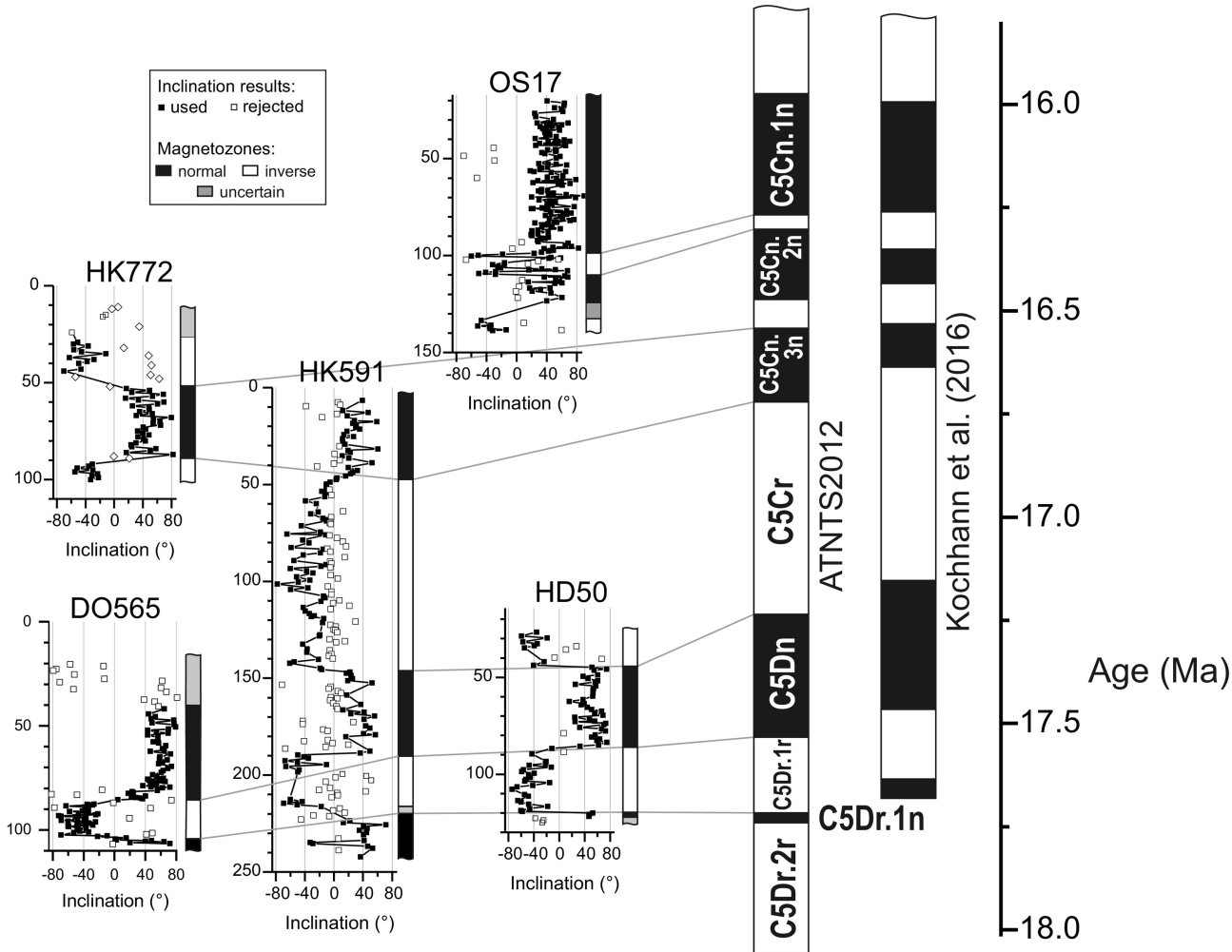


Figure 5

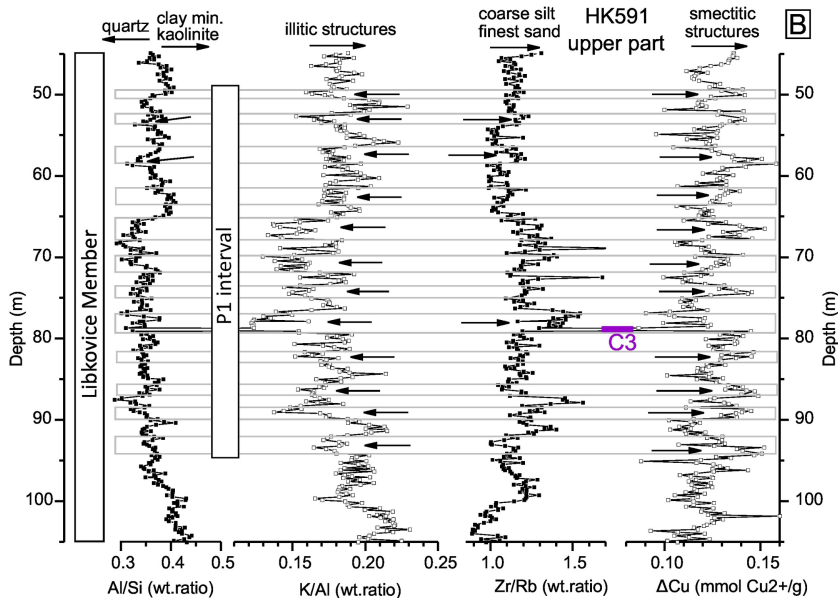
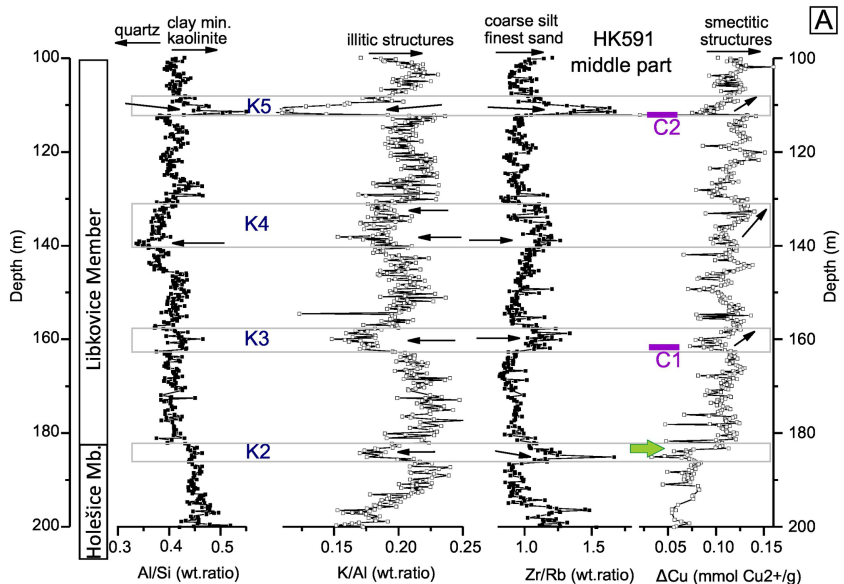


Figure 6ab

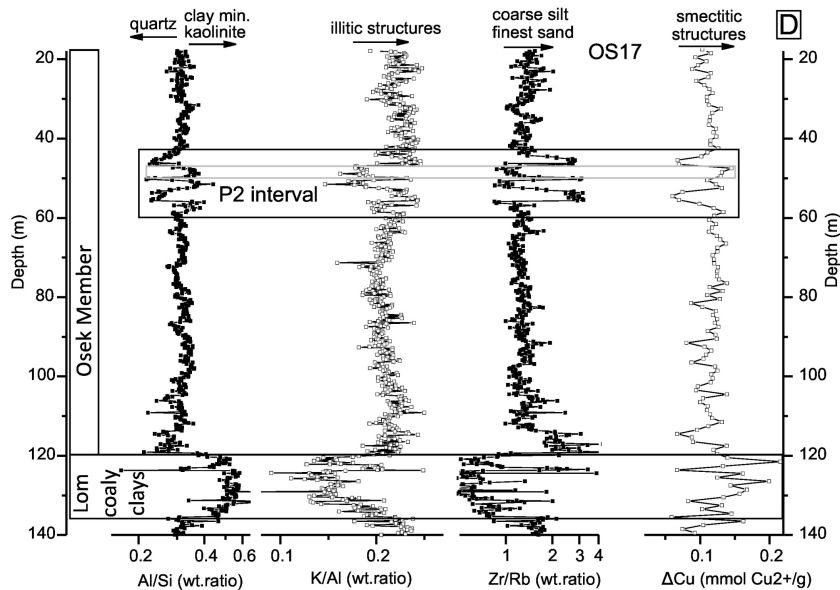
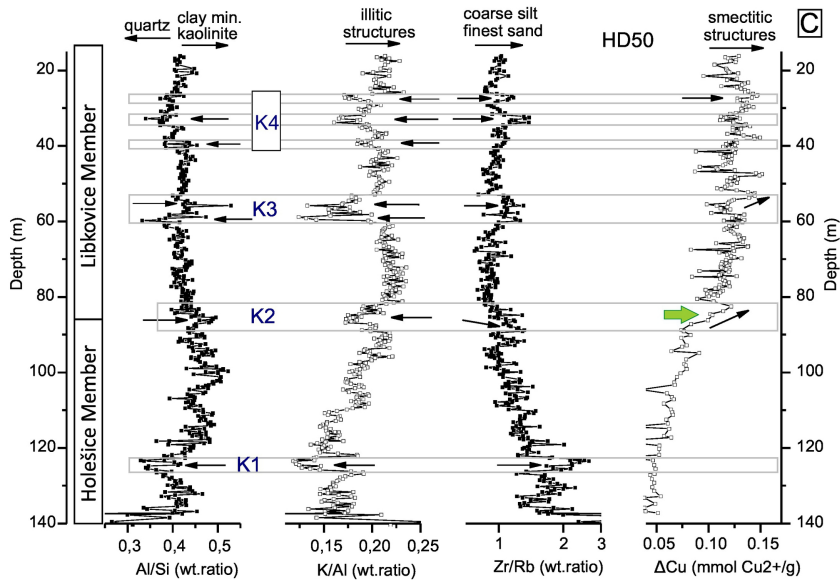


Figure 6cd

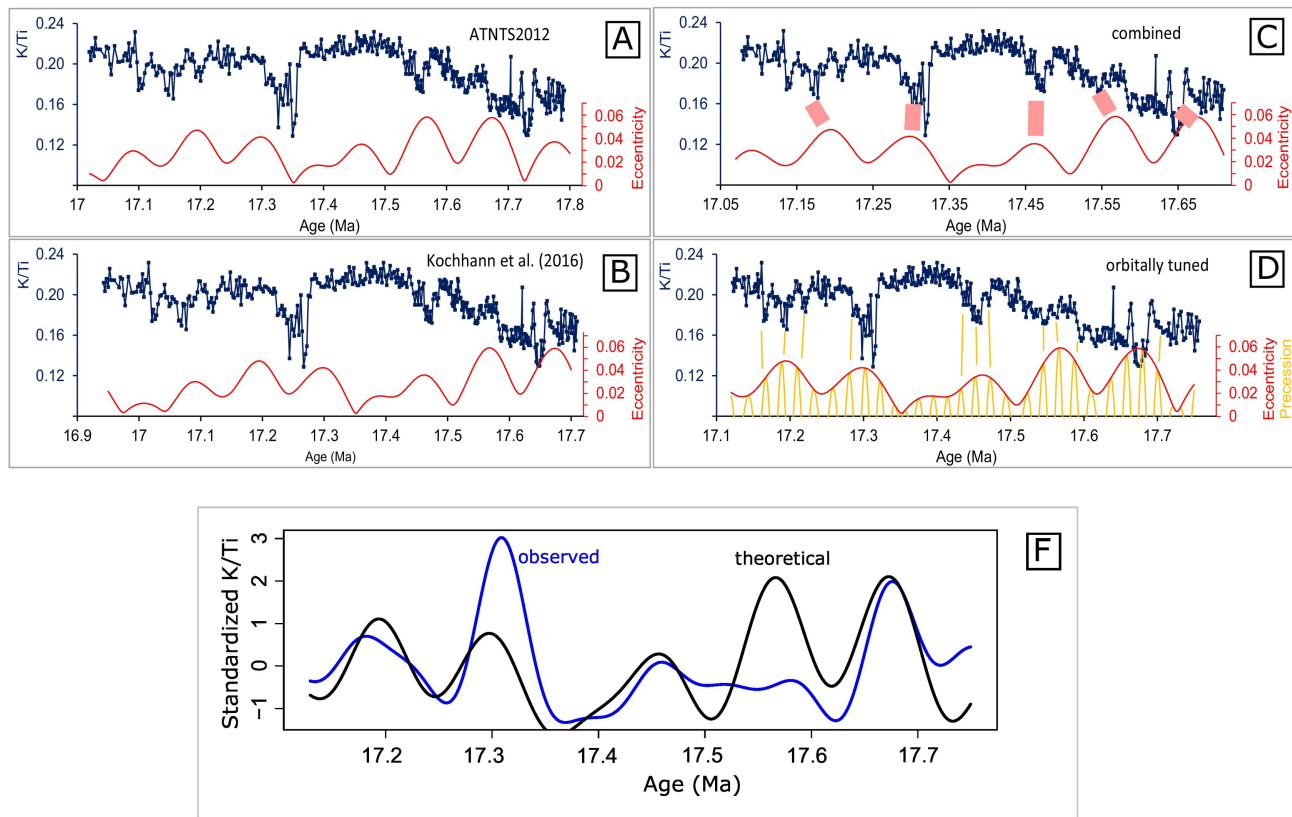


Figure 7

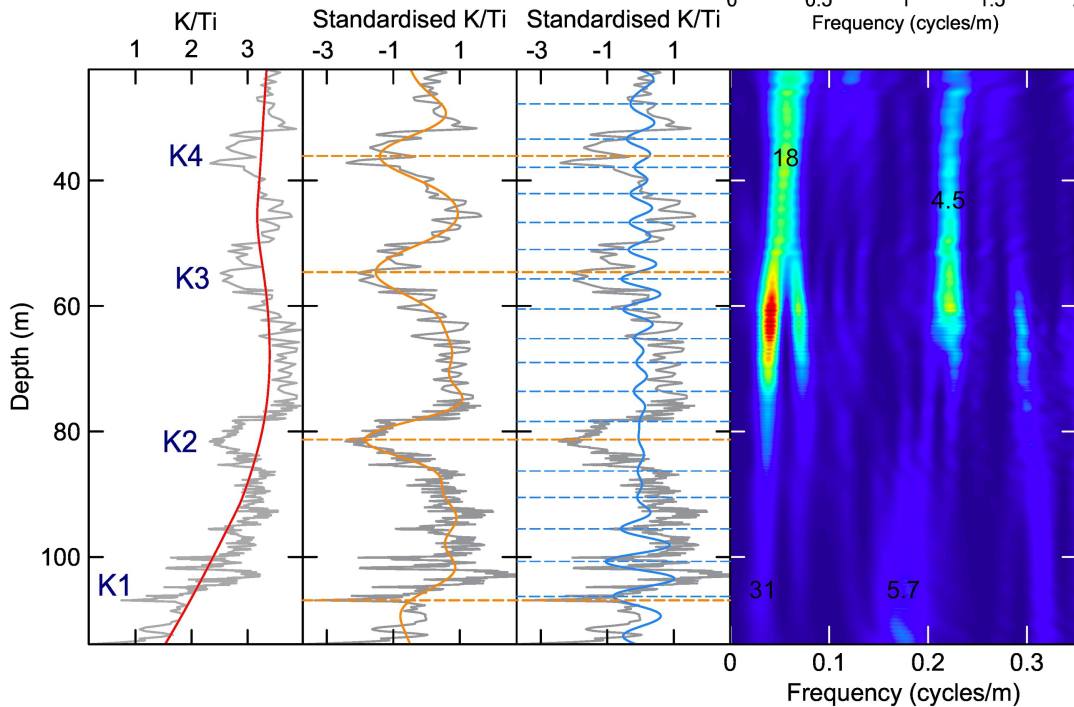
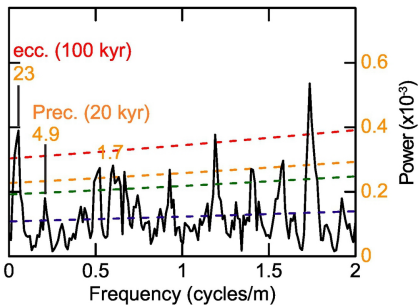
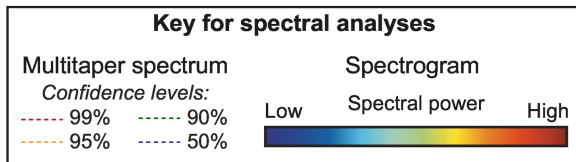


Figure 8

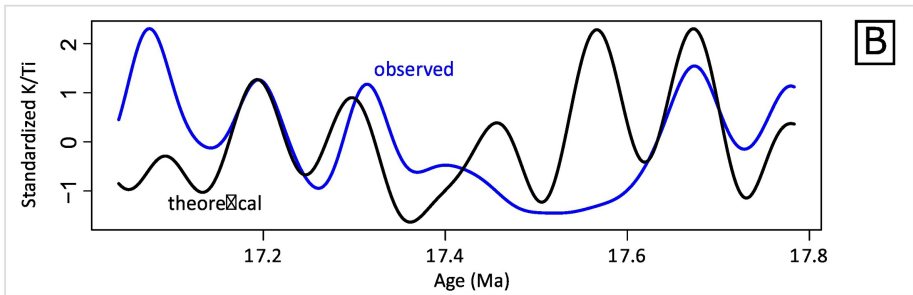
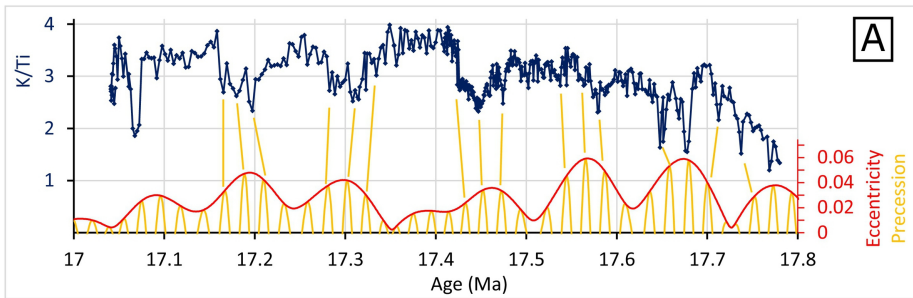


Figure 9

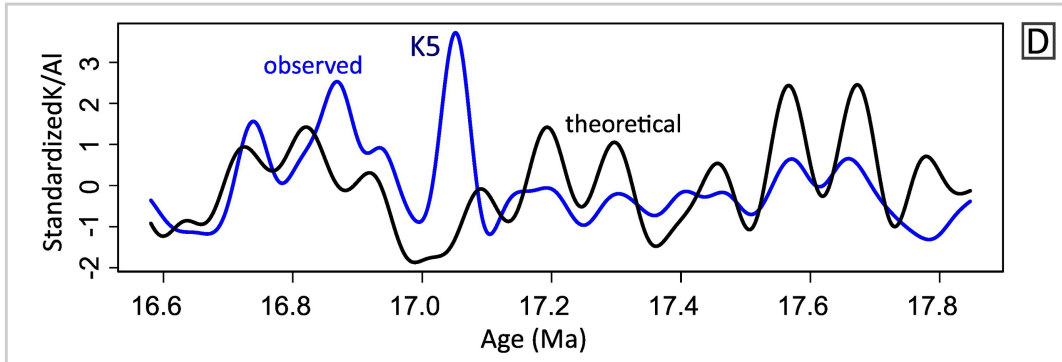
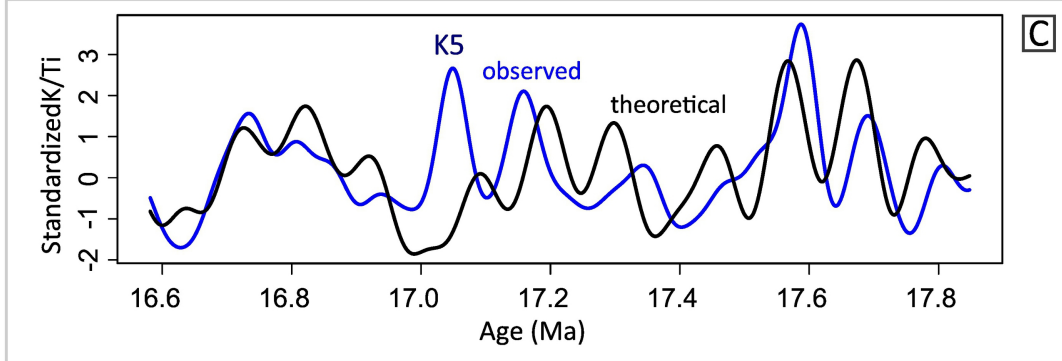
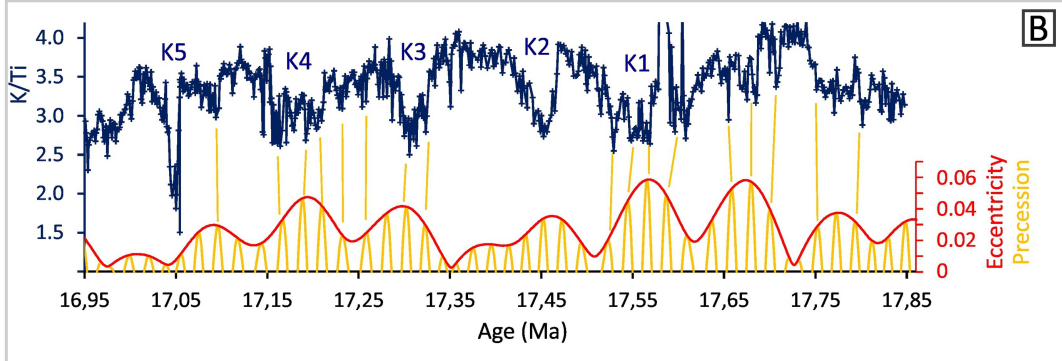
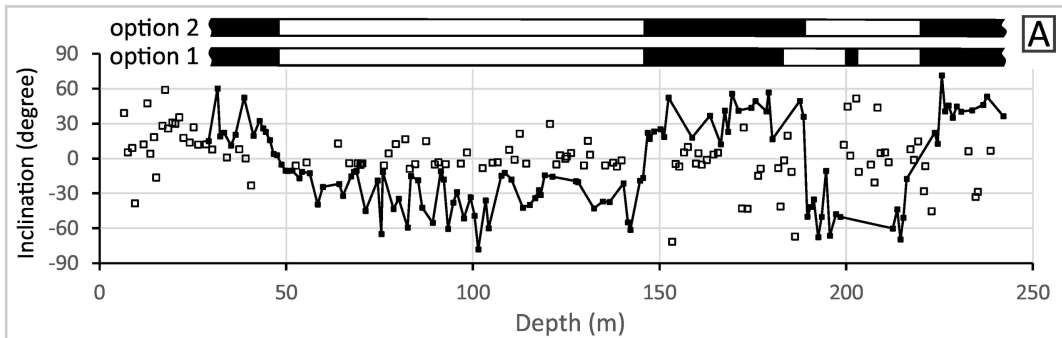


Figure 10

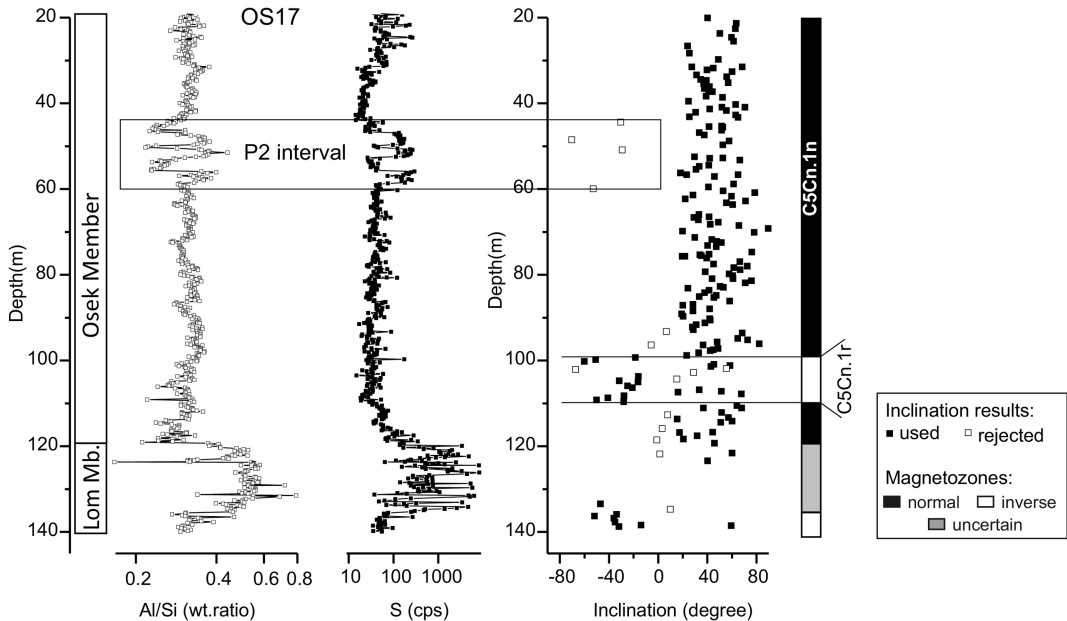


Figure 12

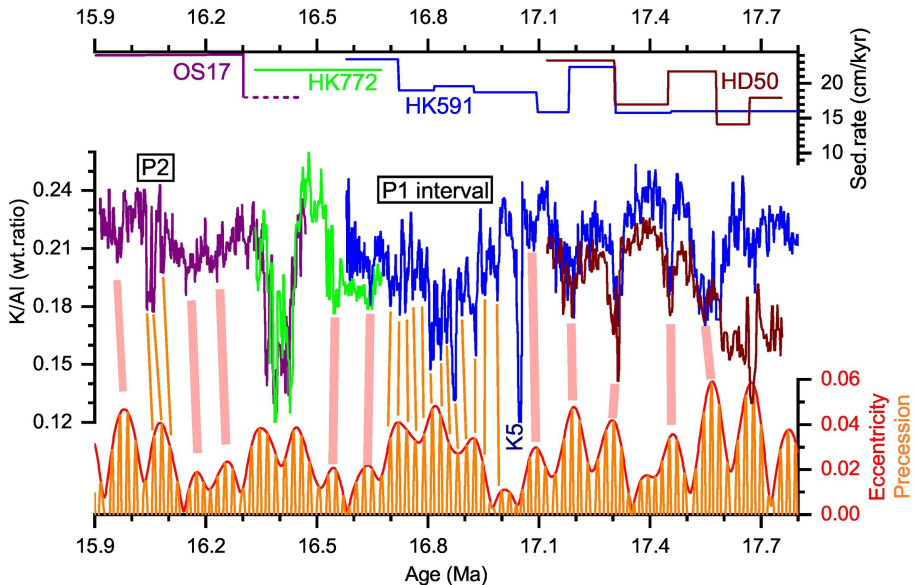


Figure 13

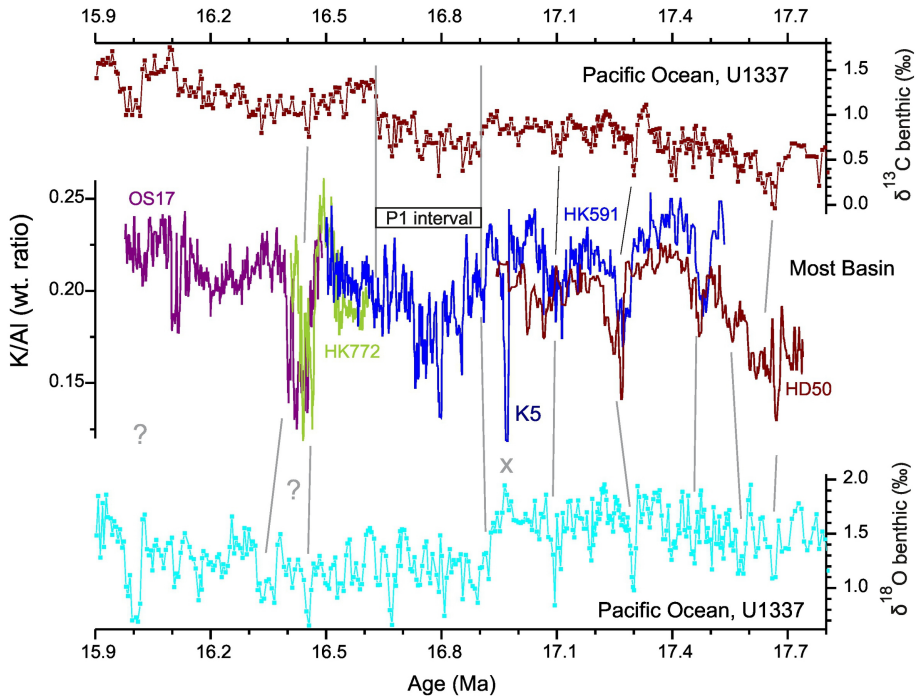


Figure 14